A HEAT CONDUCTION MODEL FOR STUDYING TRANSIENT PRESSURE BEHAVIOR IN A HOMOGENEOUS, ISOTROPIC PETROLEUM RESERVOIR

A Thesis

Presented to

the Faculty of the

Department of Chemical-Petroleum Engineering

University of Houston

Houston, Texas

In Partial Fulfillment

of the Requirements for the Degree

Master of Science in Petroleum Engineering

---

by

Allen W. Cecil

May, 1969

ACKNOWLEDGMENTS

The author wishes to express his appreciation to the following individuals and organization for their contribution to this thesis:

Professor M. G. Hubbard for his invaluable direction and advice, without which this thesis could not have been completed.

Mr. Roy Priest of the Chemical-Petroleum Engineering Department machine shop for his assistance in preparing various items for the experimental apparatus.

The Chemical-Petroleum Engineering Department for a Departmental Fellowship for the year 1967-68.

A HEAT CONDUCTION MODEL FOR STUDYING TRANSIENT PRESSURE BEHAVIOR IN A HOMOGENEOUS, ISOTROPIC PETROLEUM RESERVOIR

An Abstract of a Thesis

Presented to

the Faculty of the

Department of Chemical-Petroleum Engineering

University of Houston

Houston, Texas

In Partial Fulfillment

of the Requirements for the Degree

Master of Science in Petroleum Engineering

---

by

Allen W. Cecil

May, 1969

ABSTRACT

The mathematical description of the transient temperature behavior in a homogeneous, isotropic heat conducting medium containing a cylindrical heat source is analogous to the mathematical description of transient pressure behavior in a homogeneous, isotropic petroleum reservoir.

A heat conduction analogue was developed to experimentally verify ideal mathematical solutions for the transient reservoir pressure behavior of various geometrical systems.

The results obtained from this model provide quantitative verification of the mathematical solutions.

TABLE OF CONTENTS

CHAPTER PAGE

I. INTRODUCTION 1

II. THEORETICAL BACKGROUND 3

Transient Fluid Flow in Homogeneous,

Isotropic Porous Media 3

Governing Differential Equation 3

Solution 5

Application to Physical Systems 7

180° Fault 7

90° Fault 10

Closed System 13

Transient Heat Conduction in Homogeneous,

Isotropic Solids 17

Governing Differential Equation 17

Solution 19

Application to Physical Systems 20

180° Adiabatic Boundary 21

90° Adiabatic Boundary 22

Closed System 23

III. TRANSIENT HEAT CONDUCTION MODEL 24

Design Considerations 24

Conducting Material 24

Heat Losses 26

CHAPTER PAGE

Heating System 27

Thermocouple System 28

Description of Heat Conduction Model and

Related Equipment 29

Operating Procedure 33

IV. DISCUSSION OF EXPERIMENTAL RESULTS 34

Closed System 35

90^{o} Adiabatic Boundary 43

180^{o} Adiabatic Boundary 52

V. CONCLUSIONS AND RECOMMENDATIONS 58

BIBLIOGRAPHY 63

APPENDIX 65

A. Physical Properties 66

B. Experimental and Calculated Data 67

C. Nomenclature 80

LIST OF FIGURES

FIGURE		PAGE
1.	Volume Element	3
2.	180^{o} Fault System	8
3.	Image System for 180^{o} Fault	9
4.	Pressure Drawdown Curve for 180^{o} Fault	11
5.	90^{o} Fault System	12
6.	Image System for 90^{o} Fault	14
7.	Pressure Drawdown Curve for 90^{o} Fault	15
8.	Closed System - Well Enclosed by Three Intersecting Faults	16
9.	Pressure Drawdown Curve for Closed System . .	18
10.	Closed System Model Geometry	36
11.	Closed System Model Experimental Results . . .	37
12.	90^{o} Adiabatic Boundary Model Geometry - Case No. 1	44
13.	90^{o} Adiabatic Boundary Model No. 1 Experimental Results - A	46
14.	90^{o} Adiabatic Boundary Model No. 1 Experimental Results - B	47
15.	90^{o} Adiabatic Boundary Model Geometry - Case No. 2	50
16.	90^{o} Adiabatic Model No. 2 Experimental Results	51

FIGURE PAGE

17. 180° Adiabatic Boundary Model Geometry - Case No. 1 53

18. 180° Adiabatic Boundary Model No. 1 Experimental Results 54

19. 180° Adiabatic Boundary Model Geometry - Case No. 2 56

20. 180° Adiabatic Boundary Model No. 2 Experimental Results 57

CHAPTER I

INTRODUCTION

One of the major factors influencing the economics of the oil and gas industry is the expense of developing new petroleum reserves which results primarily from the uncertainty associated with such parameters as bulk volume, porosity, and permeability of a particular reservoir. One of the analytical techniques applied by petroleum engineers to accurately determine these parameters and reduce risks associated with developing new reserves is transient pressure analysis. The application of transient pressure analysis can result in the determination of reservoir boundaries, reservoir properties such as permeability, and the evaluation of formation damage or stimulation.

The pressure tests conducted to measure transient pressure behavior are termed pressure buildup or pressure drawdown tests, corresponding to a buildup in pressure or a reduction in pressure. These flow tests can be visualized as a step change in the producing rate from the assumed ideal steady-state reservoir conditions, i.e., either no fluid flow from a reservoir or fluid flow at a constant stabilized rate, which results in a period of transient fluid flow depending on several factors.

The equations presented and used in this work for the analysis of transient pressure behavior were developed by the late Professor P. J. Jones. The purpose of this research was to experimentally verify Professor Jones' mathematical solutions for specific idealized cases as derived for transient fluid flow with a transient heat conduction model.

CHAPTER II

THEORETICAL BACKGROUND

Transient Fluid Flow in Homogeneous, Isotropic Porous Media.

Governing Differential Equation. A mathematical description of fluid flow in porous media can be obtained by combining the following physical principles: (1) law of conservation of mass (2) Darcy's law and (3) an equation of state.

Consider fluid flow only in the x-y plane as shown in the volume element in Figure 1.

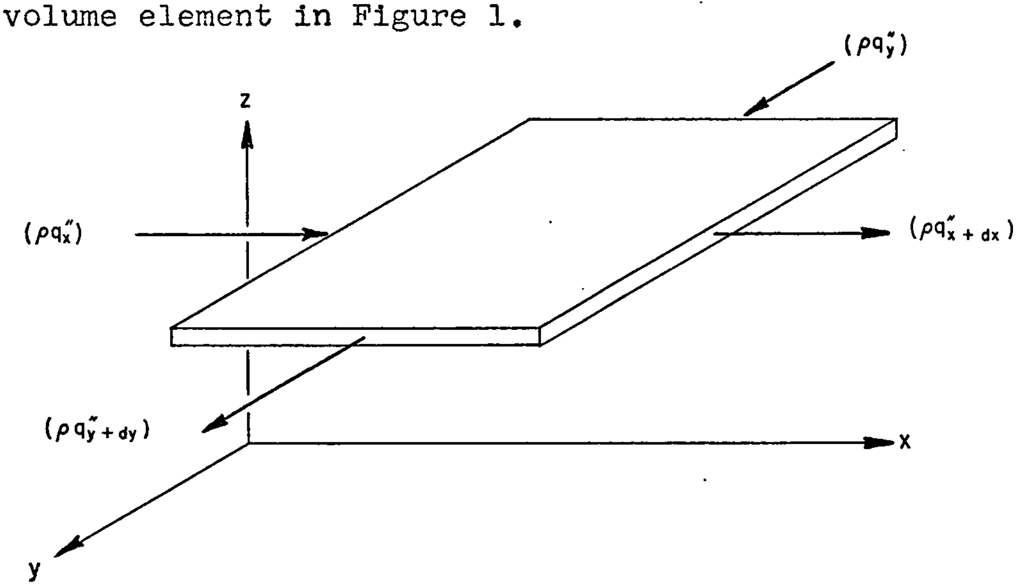

Figure 1. Volume Element

A mass balance around the volume element results in the continuity equation for the flow of fluids in porous media.

$$\frac{\partial}{\partial x}(\rho q_x'') + \frac{\partial}{\partial y}(\rho q_y'') = -\frac{\partial}{\partial t}(\rho\Phi) \qquad \text{(II-1)}$$

The flow law applicable to porous media is Darcy's Law and this law for flow in the x-direction yields

$$q_x'' = \frac{q_x}{A} = \frac{1.127}{\mu} k_x \left(-\frac{\partial j}{\partial x}\right) \qquad \text{(II-2)}$$

Assuming isothermal flow of a single-phase fluid of small and constant compressibility results in the following equation of state:

$$\rho = \rho_o e^{c(P-Pi)} = \rho_o e^{c(-j)} = \rho_o(1-cj) \qquad \text{(II-3)}$$

$$\text{for } cj \ll 1.0$$

Substitution of Darcy's Law and the equation of state into the continuity equation results in the following differential equation

$$\frac{\partial^2 j}{\partial x^2} + \frac{\partial^2 j}{\partial y^2} = \frac{1}{\eta}\frac{\partial j}{\partial t} \qquad \text{(II-4)}$$

assuming that the permeability is constant and isotropic, that the porosity is constant and that the resulting flow is laminar or viscous. Converting equation (II-4) to radial form using the substitution $r^2 = x^2 + y^2$ yields

$$\frac{\partial^2 j}{\partial r^2} + \frac{1}{r}\frac{\partial j}{\partial r} = \frac{1}{\eta}\frac{\partial j}{\partial t} \qquad \text{(II-5)}$$

This is the diffusivity equation in radial form which governs the flow of slightly compressible fluids in homogeneous, isotropic porous media.

Solution. During the early producing time of practical interest, the pressure behavior is essentially that of a radially infinite fluid reservoir. Therefore, the transient solution of equation (II-5) corresponds to the solution for a reservoir of infinite extent.

Consider a well completed in an infinitely extended homogeneous, isotropic reservoir producing at a constant reservoir volumetric flow rate, q. Carslaw and Jaeger (2:261) have shown that the solution to the diffusivity equation for a line source is

$$j = \frac{Dq}{2} \int_u^{\infty} \frac{e^{-v}}{v}\, dv = \frac{D}{2} q \left[-E_i(-u) \right] \qquad \text{(II-6)}$$

where

$u = \frac{r^2}{4\eta t}$ and $E_i(-u)$ is the exponential integral.

Defining the well function, $W(u)$, as being identically equal to the negative of the exponential integral,

$$W(u) \equiv -E_i(-u)$$

and expanding the exponential integral in an infinite series results in

$$W(u) = -\gamma - \ln u + u - \frac{u^2}{4} + \dots\dots\dots + \frac{(-1)^{n-1} u^n}{n \cdot n!} + \dots\dots\dots$$

where γ is Euler's constant.

It is convenient for practical use to reduce the well function to the logarithimic form. Except for the first two terms, all the terms of the series expansion of W(u) can be neglected for values of the argument, u, less than .01. This yields

$$W(u) = \ln\left(\frac{1}{u}\right) - 0.5772 \ , \quad u \leqslant 0.01$$

Converting the logarithm to the base 10 and substituting the well function for the exponential integral yields

$$j = 1.15\, Dq \log \frac{2.25\eta t}{r^2} \quad , \quad \frac{r^2}{4\eta t} \leqslant 0.01 \qquad \text{(II-7)}$$

For the drawdown at the well, j_W, called the self-drawdown, equation (II-7) becomes

$$j_w = 1.15\, Dq \log \frac{2.25\eta t}{r_w^2} \qquad \text{(II-8)}$$

Equation (II-8) represents the pressure drawdown for a well producing at a constant reservoir flow rate, q, from an infinitely extended homogeneous, isotropic reservoir.

It is evident from examination of equation (II-7) that a plot of j vs logt will result in a straight line of constant slope, m, equal to 1.15 Dq.

Application to Physical Systems.

The physical systems of interest in this thesis are those systems involving no-flow boundaries of varying geometry. These systems that are not infinite in extent can be solved by using the method of images and the Theorem of Superposition.

180^{o} Fault. Consider a system of one producing well located near a linear sealing fault as shown in Figure 2. The fault is a no-flow boundary and its physical presence can be replaced by the image system shown in Fig. 3. In Fig. 3, an image well, producing at the same rate as the producing well, is located by reflection across the position of the fault line. This creates a no-flow boundary at the position of the fault. The flowing pressure difference in the producing well will now be the sum of the self-drawdown (or buildup), j_w, and the interference drawdown, j_i, from the image well located at a distance of $r = 2d$ feet away. This expression is

$$j = j_w + j_i = m \log \frac{2.25\eta t}{r_w^2} + \frac{m}{2.3} W\left(\frac{(2d)^2}{4\eta t}\right) \qquad \text{(II-9)}$$

for $\frac{r_w^2}{4\eta t} \leqslant 0.01$. When $\frac{d^2}{\eta t} \leqslant 0.01$, the equation can be rewritten as

$$j = m\left(\log \frac{2.25\eta t}{r_w^2} + \log \frac{2.25\eta t}{(2d)^2}\right)$$

which simplifies to

$$j = 2m \log \frac{2.25\eta t}{2dr_w} \qquad \text{(II-10)}$$

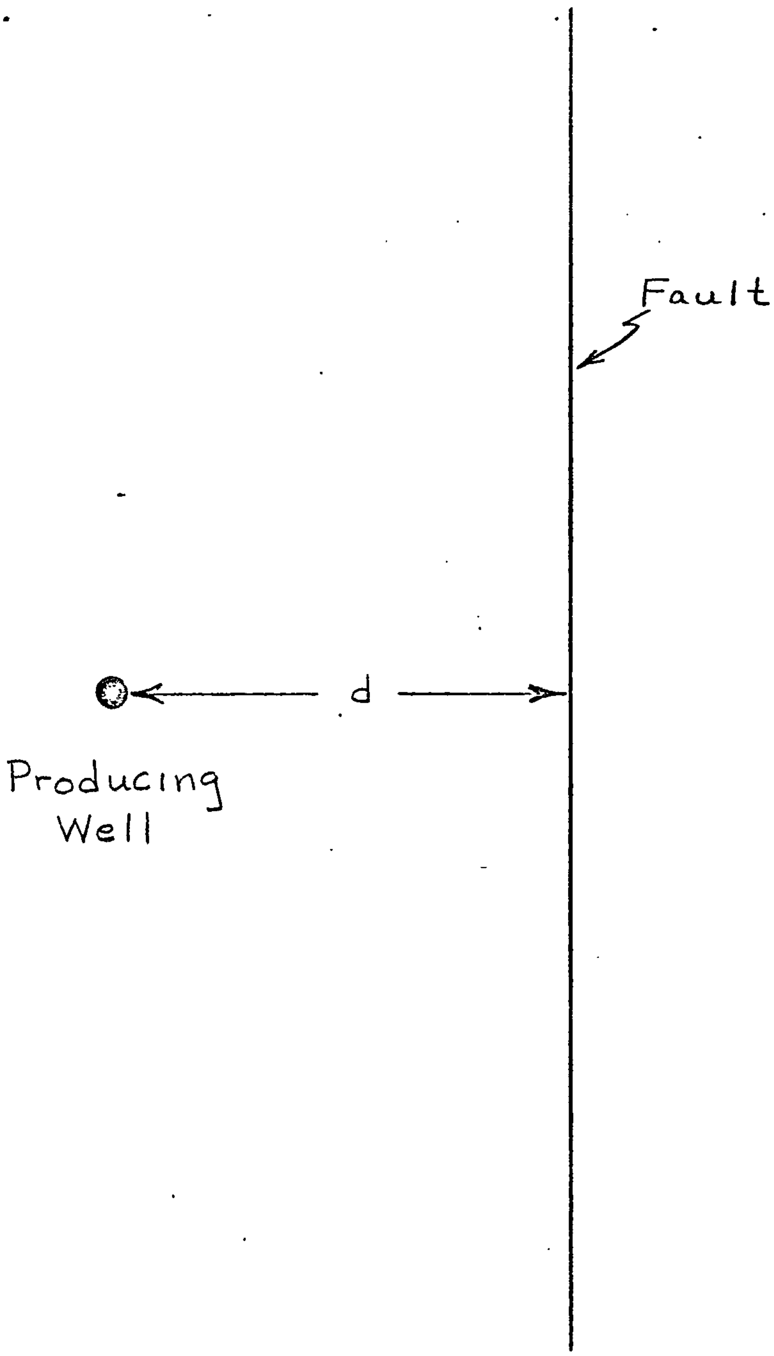

Figure 2. 180° Fault System

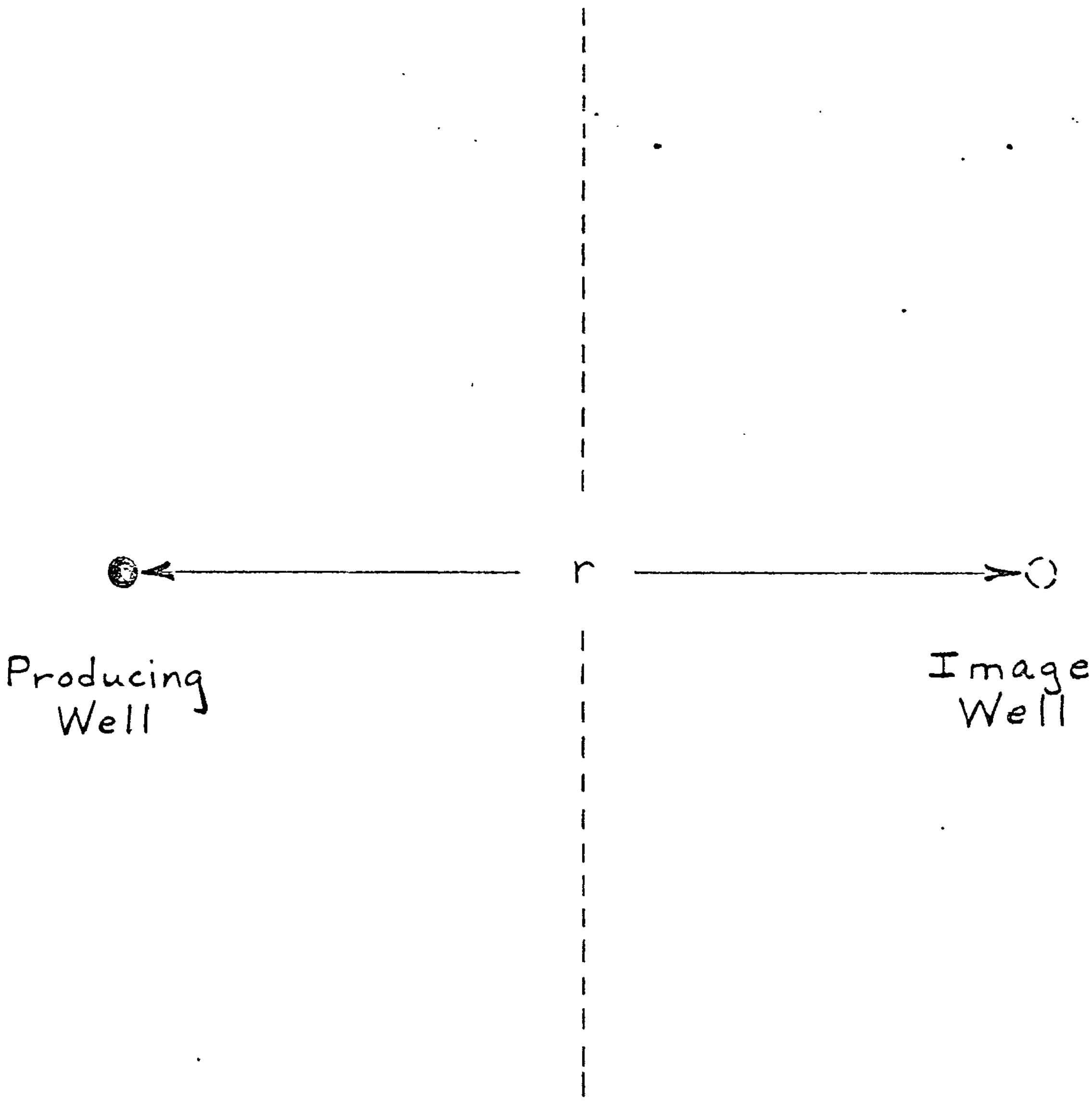

Figure 3. Image System for 180° Fault

From equation (II-10) it can be seen that a sealing fault located a distance d from the producing well causes the slope of the drawdown curve to double for large enough values of time.

A typical plot of j vs. logt for the linear sealing fault system is shown in Fig. 4. From Fig. 4, it is possible to calculate the distance to the fault. This can be done by noting the value of time, t_o , at the intersection of the two straight line portions of the drawdown curve. At this point, the drawdown predicted by equation (II-9) is equal to the drawdown predicted by equation (II-10). Equating these two equations and solving for d yields

$$d = 0.75\sqrt{\eta t_o} \qquad \text{(II-11)}$$

If the value of η is unknown, it can be determined from Figure 4. Extrapolation of the first straight line portion of the drawdown curve to j = o yields the value of time, θ, at which equation (II-9) equals zero. Equating equation (II-9) to zero and solving for η yields

$$\eta = \frac{r_w^2}{2.25\theta} \qquad \text{(II-12)}$$

<u>90^o Fault</u>. Consider the case where a producing well is located inside a 90^o fault block as shown in Figure 5. The image well system which creates the no-flow boundaries identical to those of the 90^o fault block system is shown

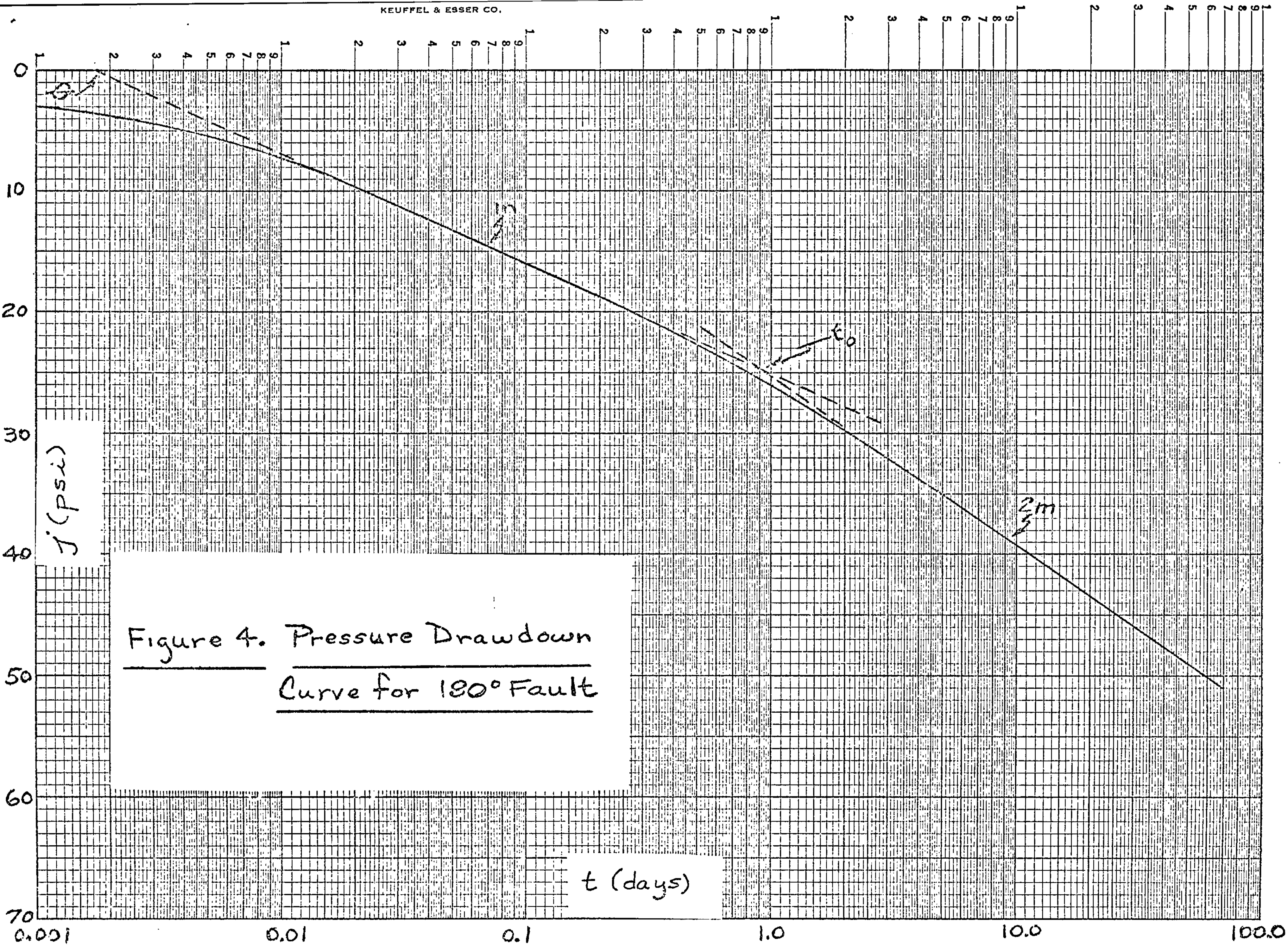

Figure 4. Pressure Drawdown Curve for 180° Fault

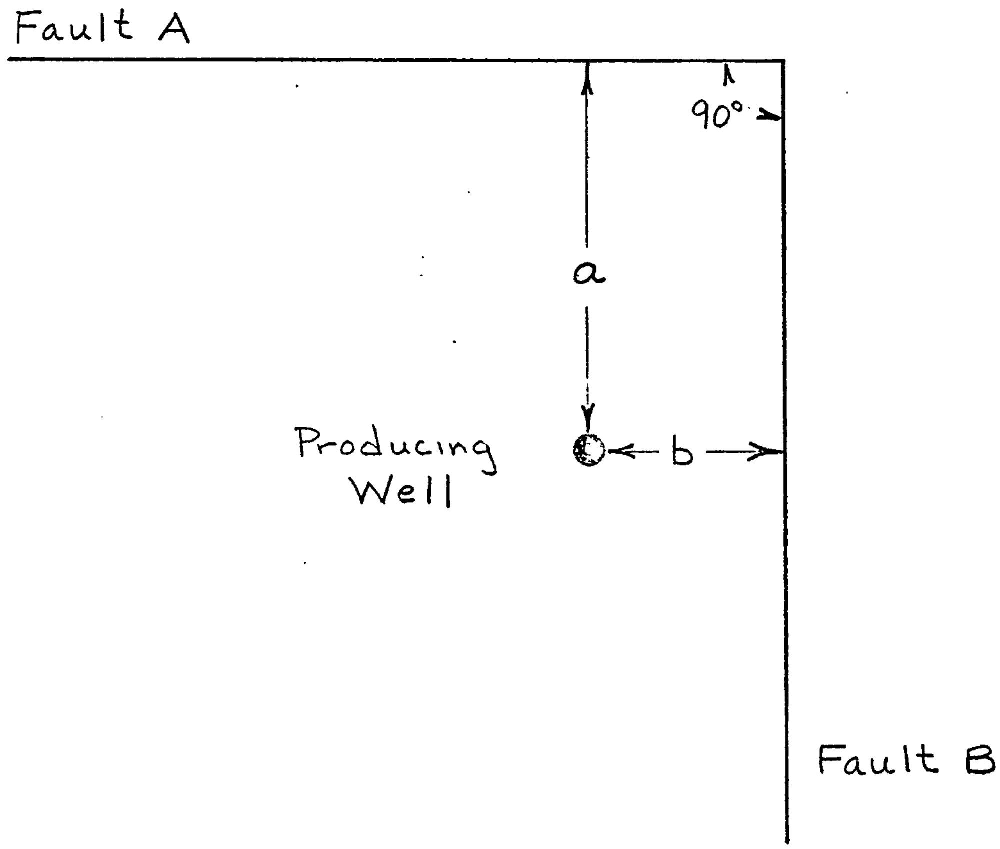

Figure 5. 90° Fault System

in Figure 6, with the image wells denoted by i_1, i_2 and i_3 When these image wells are placed on production at the same time and rate as the producing well, this system yields the same results as the original faulted system. The drawdown in the producing well is the sum of the self-drawdown, j_w, plus the three interference drawdowns of the image wells.

$$j = j_w + j_{i_1} + j_{i_2} + j_{i_3} = \frac{Dq}{2}\left[W(u_w) + W(u_{i_1}) + W(u_{i_2}) + W(u_{i_3}) \right]$$

or

$$j = \frac{Dq}{2}\left[W\left(\frac{r_w^2}{4\eta t}\right) + W\left(\frac{(2a)^2}{4\eta t}\right) + W\left(\frac{(2b)^2}{4\eta t}\right) + W\left(\frac{\left(\sqrt{4a^2+4b^2}\right)^2}{4\eta t}\right) \right] \qquad \text{(II-13)}$$

As the arguments of the well functions successively become less than 0.01, the slope of the drawdown curve will change progressively from m to 2m to 3m to 4m. The final equation in logarithm form is

$$j = 4m \log \frac{2.25\eta t}{\left[(8abr_w)^2 (a^2 + b^2)\right]^{1/4}} \qquad \text{(II-14)}$$

Figure 7 illustrates the drawdown curve from the 90° fault case. From Fig. 7, the value of η and the distances to the faults can be determined as in the linear fault case.

Closed System. A closed or volumetric reservoir is a reservoir that is completely bounded on all sides by no-flow boundaries. An example of this type of reservoir would be a fault block bounded by three intersecting sealing faults, as in Figure 8.

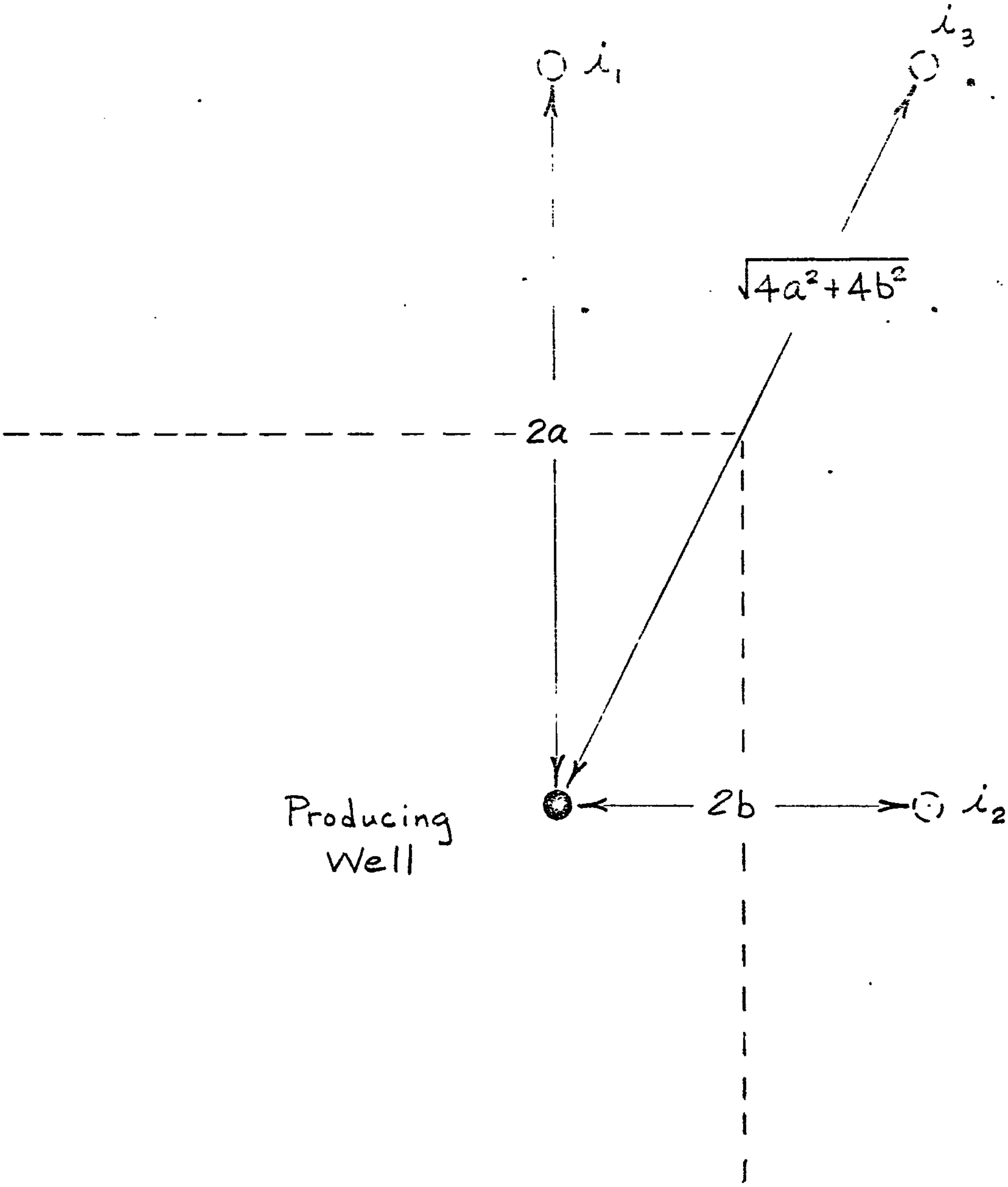

Figure 6. Image System for 90° Fault

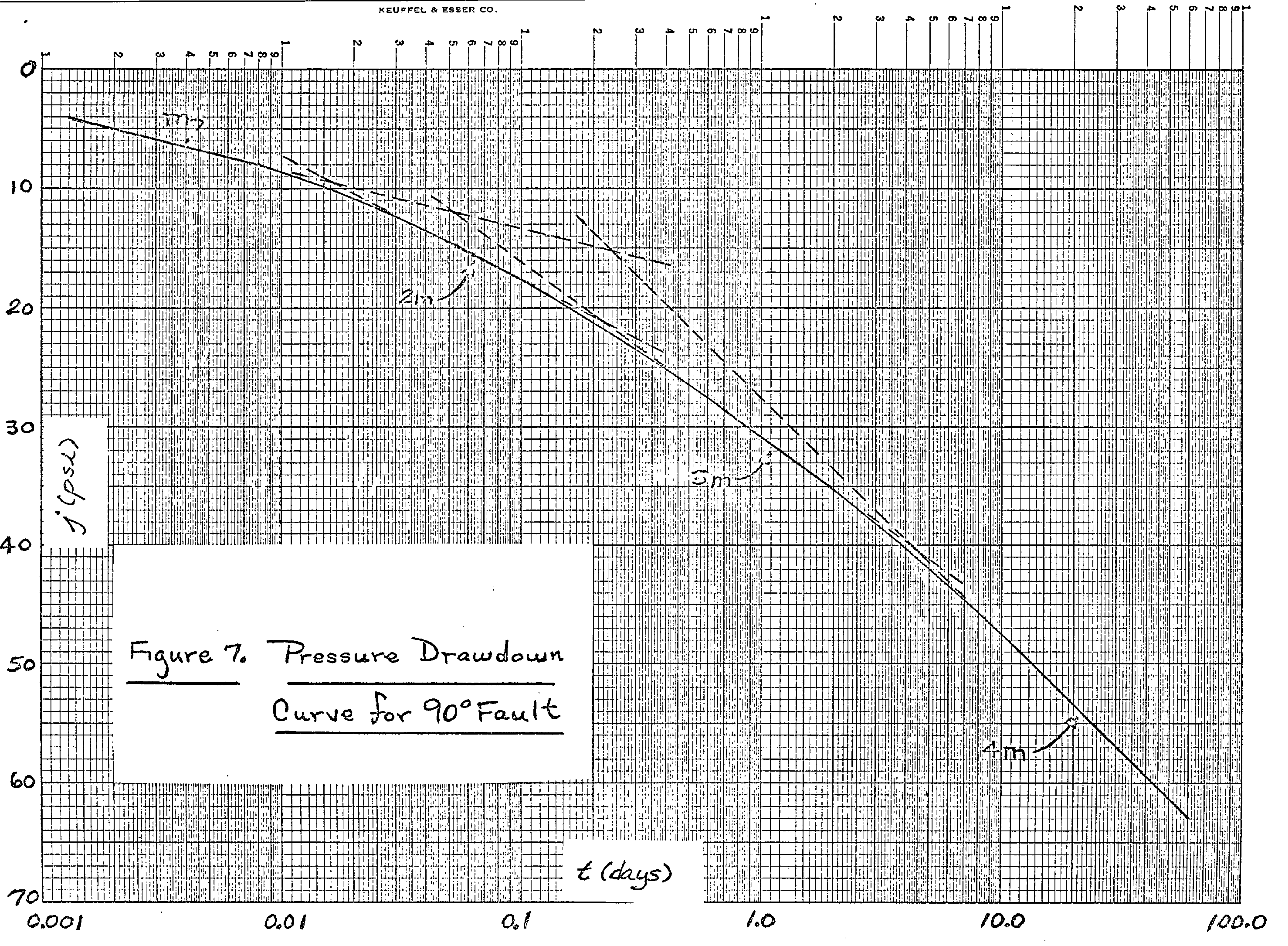

Figure 7. Pressure Drawdown Curve for 90° Fault

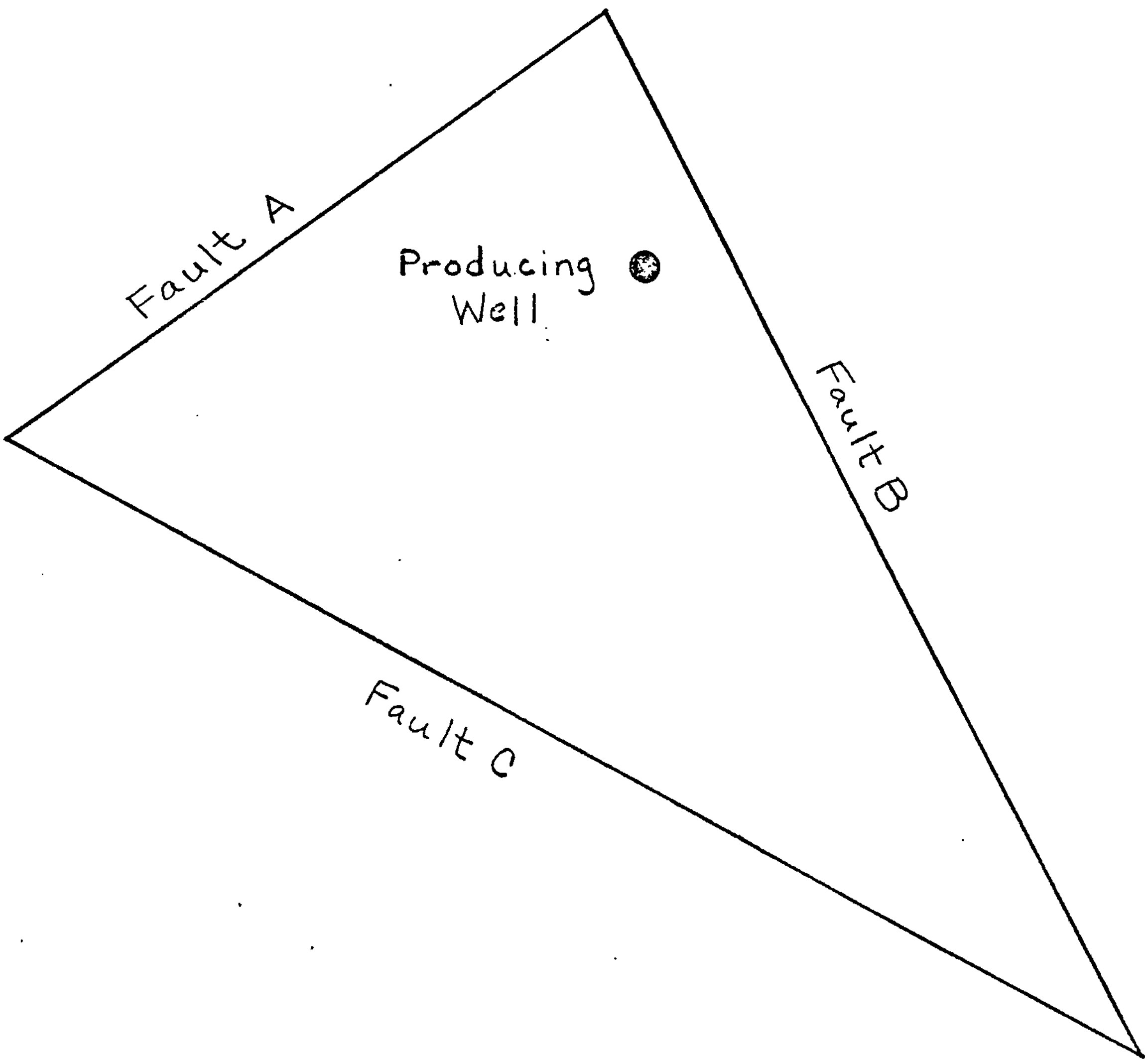

Figure 8. Closed System-Well Enclosed by Three Intersecting Faults

The drawdown curve for this system is illustrated in Figure 9. As the interference from the successive faults arrives at the producing well the slope of the drawdown curve changes from m to 2m to 3m. When the interference from the last fault arrives, the reservoir is now completely bounded and begins production by steady state. The drawdown curve starts falling off rapidly and approaches a vertical line asymptotically. The drive mechanism of the reservoir is now steady state by expansion.

The appearance of the drawdown curve in Figure 9 is representative of a closed reservoir in which all boundaries are not reached simultaneously. If all boundaries are reached simultaneously, the drawdown curve would go directly from a slope of m to a constantly increasing slope.

The image system for a closed system would require an infinite number of image wells to account for the constantly increasing slope of the drawdown curve.

Transient Heat Conduction in Homogeneous, Isotropic Solids.

Governing Differential Equation. The differential equation governing the conduction of heat in homogeneous, isotropic solids can be obtained in a manner analogous to that for fluid flow. In heat conduction, the physical principles involved are conservation of energy and Fourier's law of heat conduction.

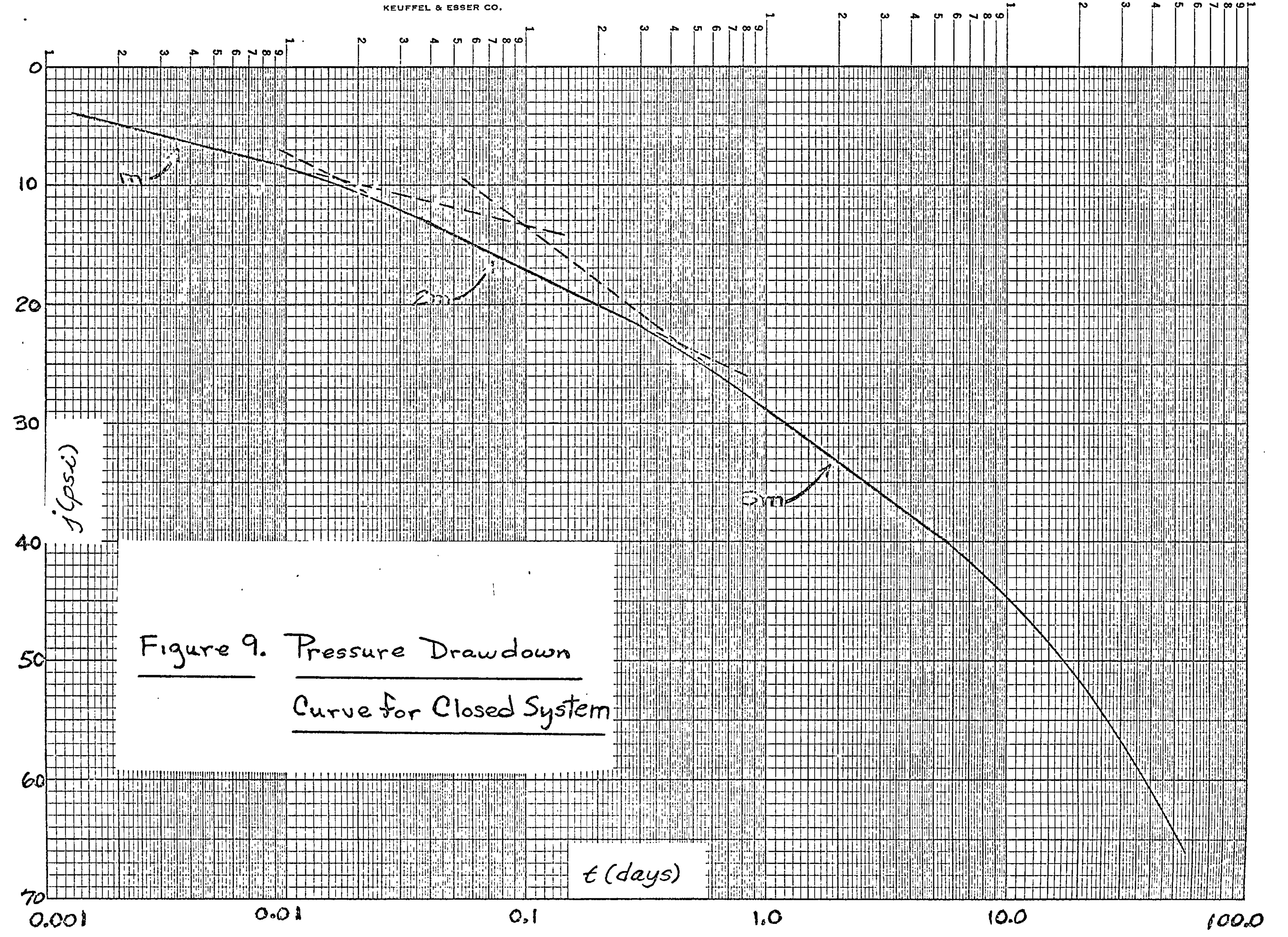

Figure 9. Pressure Drawdown Curve for Closed System

Consider a volume element such as shown in Figure 1 which is subjected to heat conduction in the x-y plane only. An energy balance around the volume element results in the following differential equation

$$\rho c_p \frac{\partial T}{\partial t} + \left(\frac{\partial f_x}{\partial x} + \frac{\partial f_y}{\partial y} \right) = 0$$

This equation corresponds to the continuity equation in fluid flow. Fourier's law of heat conduction for conduction in the x-direction yields

$$f_x = -k_x \frac{\partial T}{\partial x}$$

For a homogeneous, isotropic solid whose thermal conductivity is independent of temperature, the substitution of Fourier's law into the energy balance equation results in

$$\frac{\partial^2 T}{\partial x^2} + \frac{\partial^2 T}{\partial y^2} = \frac{1}{\alpha} \frac{\partial T}{\partial t} \qquad \text{(II-15)}$$

Converting equation (II-15) to radial form yields

$$\frac{\partial^2 T}{\partial r^2} + \frac{1}{r} \frac{\partial T}{\partial r} = \frac{1}{\alpha} \frac{\partial T}{\partial t} \qquad \text{(II-16)}$$

which is the differential equation governing heat conduction in a homogeneous, isotropic solid.

Solution. For the heat conduction problem, consider the volume element in Figure 1 with a continuous line source of constant strength, Q, parallel to the z-axis. Carslaw and Jaeger (2:261) have shown the solution to equation (II-16) for the continuous line source (or sink) to be

$$\Delta T = \frac{Q}{4\pi hk} \int_u^\infty \frac{e^{-v}}{v}\, dv = \frac{Q}{4\pi hk}\left[-E_i(-u)\right] \qquad \text{(II-17)}$$

where

$u = \frac{r^2}{4\alpha t}$ and $E_i(-u)$ is the exponential integral.

It is evident from examination of equation (II-17) that this solution corresponds to that for the fluid flow problem. Using the same development as was used for the fluid flow solution on page 3, the temperature drawdown solution can be converted to logarithmic form to yield

$$\Delta T = \frac{2.3 Q}{4\pi hk} \log \frac{2.25\alpha t}{r^2}, \quad \frac{r^2}{4\alpha t} \leqslant 0.01 \qquad \text{(II-18)}$$

For the temperature drawdown at the well, ΔT_w, (self-drawdown) equation (II-18) becomes

$$\Delta T_w = .183 \frac{Q}{hk} \log \frac{2.25\alpha t}{r_w^2} \qquad \text{(II-19)}$$

A plot of ΔT_w vs logt results in a straight line of constant slope, n , equal to $.183 \frac{Q}{hk}$.

Application to Physical Systems.

The method of application of the transient solution of the diffusivity equation for heat conduction is identical to the method used for the fluid flow case. The method of images and the Theorem of Superposition are used except that instead of sealing faults, adiabatic surfaces represent the no-flow boundaries.

Since the heat conduction solutions for the various physical systems are the same as for the fluid flow case, the following paragraphs present only the resulting equations with a minimum of explanation. Explanation and comparison of the solutions can be made by referring to the solutions for these physical systems in the fluid flow section of this chapter.

180° Adiabatic Boundary. The temperature drawdown (or buildup) in a heat source (or well) located a distance d from a linear adiabatic boundary is given by

$$\Delta T = \Delta T_w + \Delta T_i = n \log \frac{2.25\alpha t}{r_w^2} + \frac{n}{2.3} W\left[\frac{(2d)^2}{4\eta t}\right] \tag{II-20}$$

for $\frac{r_w^2}{4\alpha t} \leq 0.01$. When $\frac{d^2}{\alpha t} \leq 0.01$ the equation can be rewritten as

$$\Delta T = n\left(\log \frac{2.25\alpha t}{r_w^2} + \log \frac{2.25\alpha t}{(2d)^2}\right) \tag{II-21}$$

which can be simplified to yield

$$\Delta T = 2n \log \frac{2.25\alpha t}{2d r_w} \tag{II-22}$$

The distance to the adiabatic boundary is given by

$$d = 0.75\sqrt{\alpha t_0} \tag{II-23}$$

and the value of the thermal diffusivity is given by

$$\alpha = \frac{r_w^2}{2.25\theta} \tag{II-24}$$

The values of t_o and θ can be determined from the temperature drawdown curve as indicated in the fluid flow solution for the linear fault case.

<u>90° Adiabatic Boundary</u>. The temperature drawdown in a well located on the inside of a 90° intersection of two linear adiabatic boundaries is given by

$$\Delta T = \Delta T_w + \Delta T_{i1} + \Delta T_{i2} + \Delta T_{i3}$$

or

$$\Delta T = \frac{Q}{4\pi hk}\left[W\left(\frac{r_w^2}{4\alpha t}\right) + W\left(\frac{a^2}{\alpha t}\right) + W\left(\frac{b^2}{\alpha t}\right) + W\left(\frac{a^2+b^2}{\alpha t}\right)\right] \tag{II-25}$$

where (a) and (b) are the perpendicular distances from the well to the no-flow boundaries.

For large enough values of time, the final logarithmic form of equation (II-25) is

$$T = 4n \log \frac{2.25\alpha t}{\left[(8abr_w)^2(a^2+b^2)\right]^{1/4}} \tag{II-26}$$

Closed System. For the closed system heat conduction problem, consider a conducting solid bounded on all sides by adiabatic surfaces. An example of such a system would be a heat conduction system analogous to the closed reservoir case in fluid flow shown in Figure 8.

The character of the temperature drawdown curve for a closed system corresponds exactly to the character of the pressure drawdown curve as described in the fluid flow section.

CHAPTER III

TRANSIENT HEAT CONDUCTION MODEL

Design Considerations

Conducting Material. One of the first decisions to be made in designing a heat conduction model is that of selecting the conducting material. The major factors to be considered are (1) the thermal diffusivity of the material, (2) the ease of fabrication of models from the material and (3) the availability of the material in the desired size and shape at a reasonable cost.

The thermal diffusivity of the heat transfer medium is important in several respects. First, it is of major importance in determining the size of the model. The lower the diffusivity of the heat conducting medium, the smaller is the size of the model required for a given experiment. As model size decreases, problems of handling and insulation decrease.

Secondly, the thermal diffusivity of the conducting medium directly affects the amount and type of insulation required. Transient response of materials of high thermal diffusivity is sufficiently rapid so that a minimum of insulation is required for most cases. Materials of low thermal diffusivity, particularly those whose diffusivity is of the same order of magnitude as common insulating materials, may have significant heat losses that are all but impossible to prevent.

Thirdly, the variation of thermal diffusivity with temperature must be minimal, and the physical properties of the conducting medium must be homogeneous and isotropic.

The ease of fabrication factor involves two areas. One area of consideration is the ease of shaping the model into the required geometries. This consideration also involves the size and weight of the model since these factors would influence the ease of shaping the model.

Another ease of fabrication factor involves the method of placement of the heat "well" (source or sink) and the thermocouples. This leads directly to the problem of bonding the heating (cooling) medium to the model without introducing appreciable unwanted resistance at this interface. A similar problem exists in the placement of the thermocouples so that an intimate bond exists between the thermocouple junction and the conducting material.

The third factor in selecting the conducting material, that of cost and availability, depends to a large extent on the size of the model and is a function of the use that the material has in industrial applications. For the single-layer radial model studied in this thesis, this factor is of less importance than the other two factors in material selection.

Heat Losses. The primary factors to consider in reducing the effects of heat losses are (1) the type of insulation, (2) the duration of the test and (3) the heating (cooling) rate.

In order to prevent heat losses so serious as to invalidate the experimental work, the insulation selected should have a thermal diffusivity that is at least one order of magnitude less than the thermal diffusivity of the conducting material. The insulation should be easy to install and provide an intimate contact at the interface between the conducting medium and the insulation.

The duration of the experiment affects the heat losses in two ways. First, as the time required for a given experiment increases, the size of the model also increases. For a long time test, this can introduce a significant problem since the surface area available for heat loss is a function of the radius squared.

Secondly, short operating time allows for a maximum benefit from the contrast in transient response times between the insulation and the conducting material. This results in a minimum of the insulation being influenced by the temperature changes in the conducting material and a minimum of heat lost to heating of the insulation.

The heating rate is important in controlling heat losses from the standpoint of the temperatures involved. The higher the average temperature of the conducting medium, the greater the temperature driving force present across the insulation. An increase in the temperature driving force increases the heat losses for a given thickness of insulation.

Heating System. The heat conduction model under consideration is designed to simulate the "constant terminal rate" case of fluid flow. For heat conduction models, this case corresponds to introducing a step change in heat inflow or outflow in the heat "well" of the initially isothermal conducting medium.

One consideration of heating system design is size. The diameter of the heat well must be small in comparison to the overall dimensions of the conducting material. Such a requirement simulates actual petroleum reservoir conditions and reduces the effect of the inhomogeneities introduced into the system by the presence of the well.

A second factor in heating system design is the bonding in the well of the heater to the conducting medium. This involves the method of heater use, that is, will the heater be placed permanently or temporarily in the well. In either case, the bonding material must maintain efficient heat transfer from the heater to the conducting medium and the resistance to heat transfer of the bonding material should be small and temperature independent over the temperature range used.

A third consideration in heater design is the thermal response of the heater. For ideal conditions the heater should be able to provide instantaneously the required heating rate for a given experiment.

Two possible methods of heating (cooling) the model that fit the above constraints are electrical resistance heating and the use of a thermoelectric cooler. Electrical resistance heating would be the simplest from the standpoint of the related electronic equipment required, since the thermoelectric cooler would require a feedback control system in order to provide a constant cooling rate.

Thermocouple System. The most satisfactory temperature sensing device in models of the type under consideration is the thermocouple. The type of thermocouple material which will be most satisfactory can be determined from consideration of the temperature level and the temperature change expected when the model is operating.

The major problem in this area is the means of using the thermocouple to obtain accurate temperature difference measurements. This problem involves the position of the thermocouple with reference to the heat well so as not to introduce a significant inhomogeneity in the system at the position of the thermocouple.

Size of the thermocouple junction is also important as it relates to the position problem and as it affects thermocouple response.

Description of Heat Conduction Model and Related Equipment.

The model developed for this investigation uses aluminum as the conducting medium. The aluminum being used is aluminum alloy #5052 which has a thermal conductivity of 80 $\frac{\text{Btu}}{\text{hr-ft}^{\circ}\text{F}}$ and a thermal diffusivity of 2.08 ft^2/hr. The conducting medium is 4'x4'x1/4".

The insulation used on the model is a rigid polyurethane foam which has a thermal conductivity of 1.15×10^{-2} $\frac{\text{Btu}}{\text{hr-ft}^{\circ}\text{F}}$ and a thermal diffusivity of .029 ft^2/hr at 1 atm and 70°F. Two sheets of the foam measuring 4'4"x4'4"x3" are used to insulate the upper and lower surfaces of the conducting material. This allows for a 2" overhand of insulation completely around the conducting material. The edges of the aluminum plate are insulated by 2" wide strips of polyurethane foam pressed into the 1/4" crevice between the upper and lower sheets of the foam.

The entire model rests on 4"x4"x1/4" plywood blocks placed to provide pressure points for compressing the rigid foam closely against the aluminum plate. Plywood blocks are placed on the upper side of the model directly opposite the blocks on which the model rests. The insulation is compressed around the conducting plate using 15 lb. lead bricks at the pressure points. Several cotton strings are wrapped around the model to secure the insulation before the lead bricks are placed on the model.

Electrical resistance heating is the method used to heat the model. The heater uses a cylindrical teflon core around which resistance wire is wrapped. The one-piece heater core has two sections. The small diameter section is machined to a diameter which provides a tight fit in the heater well drilled in the aluminum plate. This section is 1/2" long. The large diameter section has a diameter twice that of the small diameter section and is 1/2" long. The 1/4" length of the small diameter section adjacent to the large diameter section is the heater section and it is threaded with 72-88 threads per inch that are .002" to .003" deep. Karma (Driver-Harris Co.) resistance wire is wrapped in the threads of the 1/4" heater section. This wire has a diameter of .0008" and a resistance of 1320 ohms per foot. The resistance wire is glued in place using Eastman 910 glue and soldered at each end of the heater section to small lead wires. The lead wires are glued in place in insets machined in the teflon core on both ends of the heater section.

This heater is designed to have a resistance of 650-700 ohms in the heater section for a diameter of 3/32" to 1/8" and to provide a heat output of 30 Btu/hr or less. The design of the heater allows the heater to be inserted in the aluminum plate like a shear pin for easy installation and removal. A non-setting silicon compound (G.C. Electronics #8101-5) is used to provide efficient heat transfer from the heater to the aluminum and to ensure electrical isolation of the heater from the aluminum plate. The heater was driven by AC or DC power supplies.

The thermocouple wire used is 30 gauge iron-constantan which has a diameter of .010". All thermocouples used in the model are placed as observation points away from the heater well. The method of installation is to drill a .015" o.d. hole completely through the aluminum plate. One wire of the thermocouple is threaded through the thermocouple hole and a small thermocouple junction is made by very careful soldering. The thermocouple bead formed is a tight fit in the .015" hole and is pulled to a position one-half way through the plate. The thermocouple wire is glued to the surface of the aluminum plate using Testor's cement.

The thermocouples used during the buildup tests used 32°F reference junctions. Two types of reference junctions were used; (1) ice bath and (2) electrical equivalent reference junction (Consolidated Ohmic Devices, Inc., model JR99D, reference temperature 32°F).

This model is designed to operate at low heat rates which create a small temperature buildup near the heat well of approximately 15°F maximum. A 15°F temperature change, measured by the iron-constantan, causes a change in the emf output of the thermocouple of approximately .45 millivolts. In order to accurately measure such a small change in thermocouple output several pieces of electronic equipment were used.

The output of the thermocouple was connected to a Dana amplifier (model 3520) where a gain of 100 was used. The amplifier output was connected to a Wavetek Dialamatic null voltmeter (model 207). The output of the voltmeter provided a gain of 28 or 280 to one for any change from null depending on which meter sensitivity was used. A Sanborne Dual Channel DC amplifier recorder was used to record the output of the voltmeter.

The electronic equipment used provided the capability of amplifying the change in thermocouple output by a factor of 28000 to one for most experimental runs. In some cases, an amplification of 2800 to one was used because of the rapid response of the thermocouple due to the relationship of the thermocouple to the heater well.

Operating Procedure.

Initially, the conducting medium is at room temperature. The voltage to be applied to the heater is set on the power supply and the output of the thermocouple is nulled on the differential voltmeter. The recorder is zeroed and the appropriate recording scale is selected. The sensitivity is selected for the voltmeter as 1% or .1% of full scale, 1 volt. The recorder paper speed is set at 20 mm/sec and the recorder is started. At the same time that the switch is thrown to apply the voltage to the heater, the marker button on the recorder is pushed marking the start of the test on the recorder strip chart.

As the temperature rises at the recording thermocouple, the thermal emf output rises causing the voltmeter to be increasing out of null. The voltmeter is successively returned to near the null position by increasing the nulling voltage in steps of 1mv or 10 mv depending on the meter sensitivity used. This process is repeated throughout the entire test.

After approximately two minutes the paper speed on the recorder is reduced to 1 mm/sec and left at this speed for the remainder of the test. Test times vary with the maximum being about two hours.

CHAPTER IV

DISCUSSION OF EXPERIMENTAL RESULTS

In this chapter the geometry for each of the model cases investigated is described along with a discussion of the experimental results obtained.

Although all tests conducted were buildup tests, i.e., temperature increasing tests, these tests are plotted as drawdown tests are normally plotted as a matter of convenience. This point is made strictly to explain the method of plotting, because the character of both types of plots is exactly the same since both drawdown and buildup are described analytically by the same equation (II-19).

All the equations derived in Chapter II, apply specifically to the arrangement where the observation point is located at the interface of the wellbore and the radius of the wellbore is small in relation to the other distances involved. This is the case for a petroleum reservoir, but as noted in Chapter III, the heat conduction models used in this work placed the observation point some distance away from the wellbore. This changes slightly the form of the equations and the required input values for r_W and the other distances involved. The exact equations used to calculate expected ideal curves for each of the geometries investigated along with the experimental and calculated data are shown in Appendix B.

Closed System.

A planer view of the closed system model used in this experimental work is illustrated in Figure 10. As described in Chapter III, the conducting medium is an aluminum (alloy #5052) plate one-quarter of an inch thick and four feet square. For the closed system case, the distance from the thermocouple well to the heater well is one inch measured center-to-center and the heater well is approximately one-eighth of an inch in diameter.

The experimental data plotted in Figure 11 along with the expected ideal curve result from a test conducted with the closed system model using the electrical thermocouple reference junction and an AC power supply to drive the one-eighth inch diameter heater. The heat rate utilized was 15.7 Btu/hr.

The experimental results illustrated compare quite favorably with the ideal curve for most values of time with the maximum deviation occurring in the early time data, that is before $3x10^{-3}$ hours. The early time data follow closely the trend of the ideal curve, but are displaced yielding values of temperature buildup ranging from fifty percent to ten percent less than the expected values. The data after

Figure 10. Closed System Model Geometry

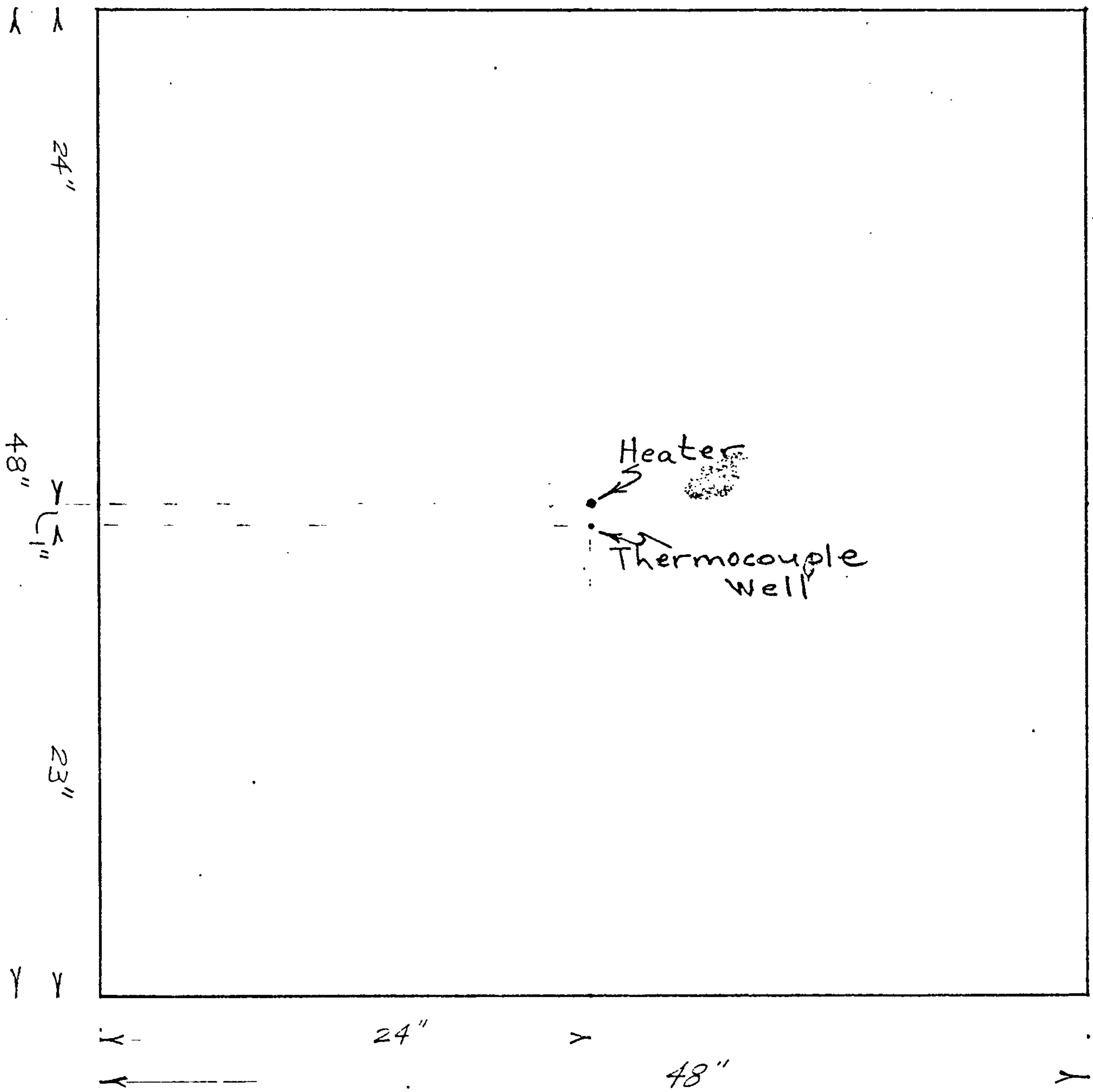

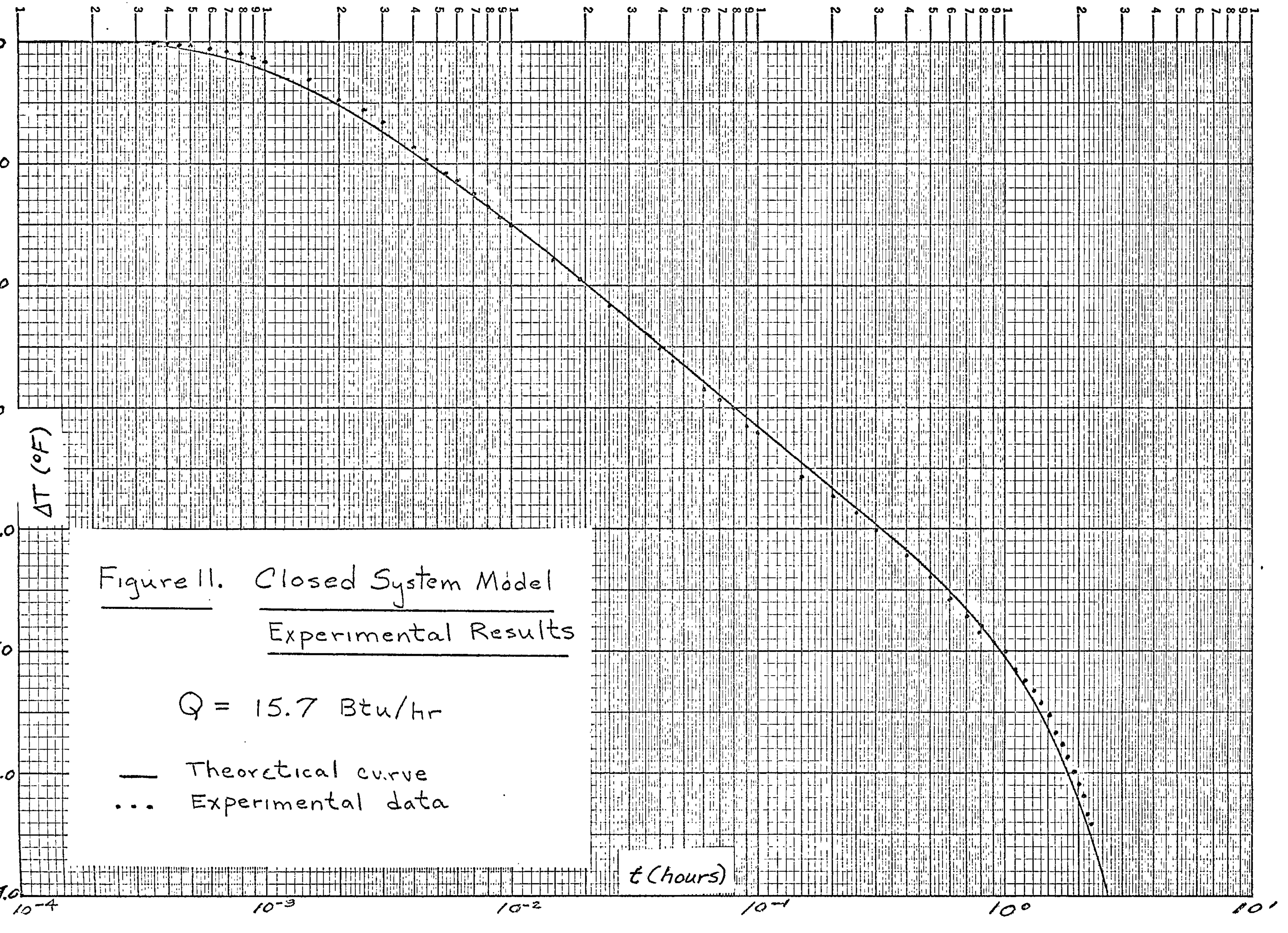

Figure 11. Closed System Model Experimental Results

$3x10^{-3}$ hours are generally within ±4% of the expected ideal values and this is definitely within the experimental accuracy expected.

In the vicinity of $8x10^{-1}$ hours, the data make a distinct jump of unusual magnitude after the data appear to have settled on a definite trend slightly below the ideal curve. After this jump the data follow closely the trend of the ideal curve eventually getting slightly above this curve. A jump similar to the one illustrated occurred in the vicinity of $8x10^{-1}$ hours every time a test was run with this model. Since this phenomenon was not reproduced in any of the other experiments using the 90° or 180° adiabatic boundary cases where the tests were run for a sufficient length of time, a reasonable explanation for this behavior would be that it was caused by a geometry effect unique to the system that was used.

The behavior of the early time data as described above could be affected by several factors. One of these factors would be heater well geometrical irregularities that cause deviations in the lines of heat flux from the ideal case. An example of such an irregularity would be the case where the geometry of the heater well was approximated more nearly by an ellipse than a circle. The resulting lines of heat flux for a uniform heat output would have a configuration unaccounted for by the mathematical model, thus causing a deviation from the assumed ideal case that would depend upon the relative positions of the heater and thermocouple wells. The effect of the relative positions of the two wells on the experimental results where wellbore irregularities existed would be two fold. First, using the ellipse example, the closer the thermocouple well is to the heater well the more the heater well appears to be an ellipse, while at larger distances the lines of heat flux would appear to be more like those of a circle. Secondly, the position of the thermocouple well with reference to the heater well irregularities would be important, since being exactly opposite an irregularity would have more effect on the lines of heat flux at the thermocouple than the same irregularity on the opposite side of the heater wellbore.

While the above discussion centered primarily on two idealized geometries, an ellipse and a circle, the geometry of any given heater well could have an irregular shape, or simply have microscopic irregularities in the wellbore surface that affect the lines of heat flux to varying degrees depending on several factors to cause deviations from the ideal case. The distortions caused by this geometry effect would be particularly important in the early time data since the magnitude of the temperature change is small and there would be no other effects to reduce their importance. For later time data, this effect should be minimized due to the greater magnitude of the temperature change and in the case where adiabatic boundary reflections of heat flux lines occur, these reflections should tend to reduce any distortions in the lines of heat flux.

Another factor affecting early time data will be the response of the thermocouple which is a function of the contact between the conducting medium and the thermocouple junction. The lack of intimate contact would cause a skin effect which would delay the response of the thermocouple to any temperature change within the conducting medium. Again this effect should cause its maximum deviation during the early time data when temperature change is small and delays in response by the thermocouple of the order of .1 to .2 of a second would be quite significant.

The above described skin could also be temperature dependent and affect temperature readings in a different way at different temperatures. Such an effect should be small in the experimental work done here since temperature changes are small in relation to the ambient temperature level and to the average temperature of any one point over the period of time that the test is run.

The behavior of late time data, i.e., data taken after the first linear slope becomes apparent, can also be affected by several factors. One of these factors would be heater wire resistance which is some function of temperature. The average temperature of the wire is expected to vary from $70^{o}F$ to a maximum estimated temperature of $300^{o}F$, and any resulting change in resistance would affect the heat output of the heater to change it from the calculated value. This effect was minimized by the use of Karma resistance wire. Karma has a temperature coefficient of resistance of $\pm 5\times10^{-6}$ $\frac{\text{ohm}}{\text{ohm}^{o}\text{C}}$ over the temperature range of interest which results in a maximum change in resistance of less than ±.1%. Such a change is definitely within experimental accuracy and should pose no problem to early or late time data.

The output of the power supply which drives the heater can have variations in output which affect the heat output experienced by the heat conducting medium. It is believed that the power supply used experienced charges in output approaching ±2%. Although this is within experimental error it definitely could affect the recorded data as observed in Figure 11.

Other possible errors in model performance stem from manufacture of the heaters, since their manufacture was difficult at best. Although a general set of specifications was applied to all heaters, their manufacture was subject to a certain lack of uniformity. An example of such a nonuniformity would be the case where the one fourth inch heater section was threaded in such a manner that one wrap or less of the heater wire was actually outside the boundaries of the heat conducting medium. It would be expected that the major portion of heat generated by any heater wire outside the heater well would be transmitted by the plate since it is by far the most heat conductive medium present. Even so this situation is not considered by the mathematics and it would represent a departure from the ideal case causing a deviation in the expected output.

The above comments represent a discussion of the mechanical, electrical, and geometrical factors which would affect the performance of the model to some degree, and it is seen that many of these effects are probably small and within experimental accuracy.

A second major area exists which can contribute significant errors and this area is that of the electronic system used to amplify and record the temperature changes experienced by the thermocouple. The maximum temperature change experienced in the closed system case was 6.5°F which results in a change of .195 millivolts in the electrical output of the thermocouple. This change represents a change of 15% above an approximate initial output of 1.30mv. Overall experimental accuracy of the order of four to five percent would be a good estimate of that expected and the above temperature change represents only a change of three to four times that accuracy. This can be significant when the time factor is considered since the fifteen percent change discussed above occurs over a 2 hour period. What about changes of the order of 3.5% which occur over thirty-six seconds? Definitely changes of this magnitude will be affected by mechanical shocks, slight but perceptible changes in room temperature affecting electronic equipment, electrical transients introduced by poor grounding techniques (example: no earth ground existed in building) and common power variations.

Although primary discussion of possible errors affecting the performance of the physical model occurs in this section on the closed system case, all the above comments apply to all the models used and the possible errors previously noted may be referred to in the discussions of the experimental results for the 90° and 180° adiabatic boundary cases.

90° Adiabatic Boundary

The geometry of the first 90° adiabatic boundary case is illustrated in Figure 12. The two adiabatic boundaries (edges of the aluminum plate) are 1.375" from the center of the heater well with the thermocouple being one-eighth of an

Figure 12. 90° Adiabatic Boundary Model Geometry-

Case No. 1

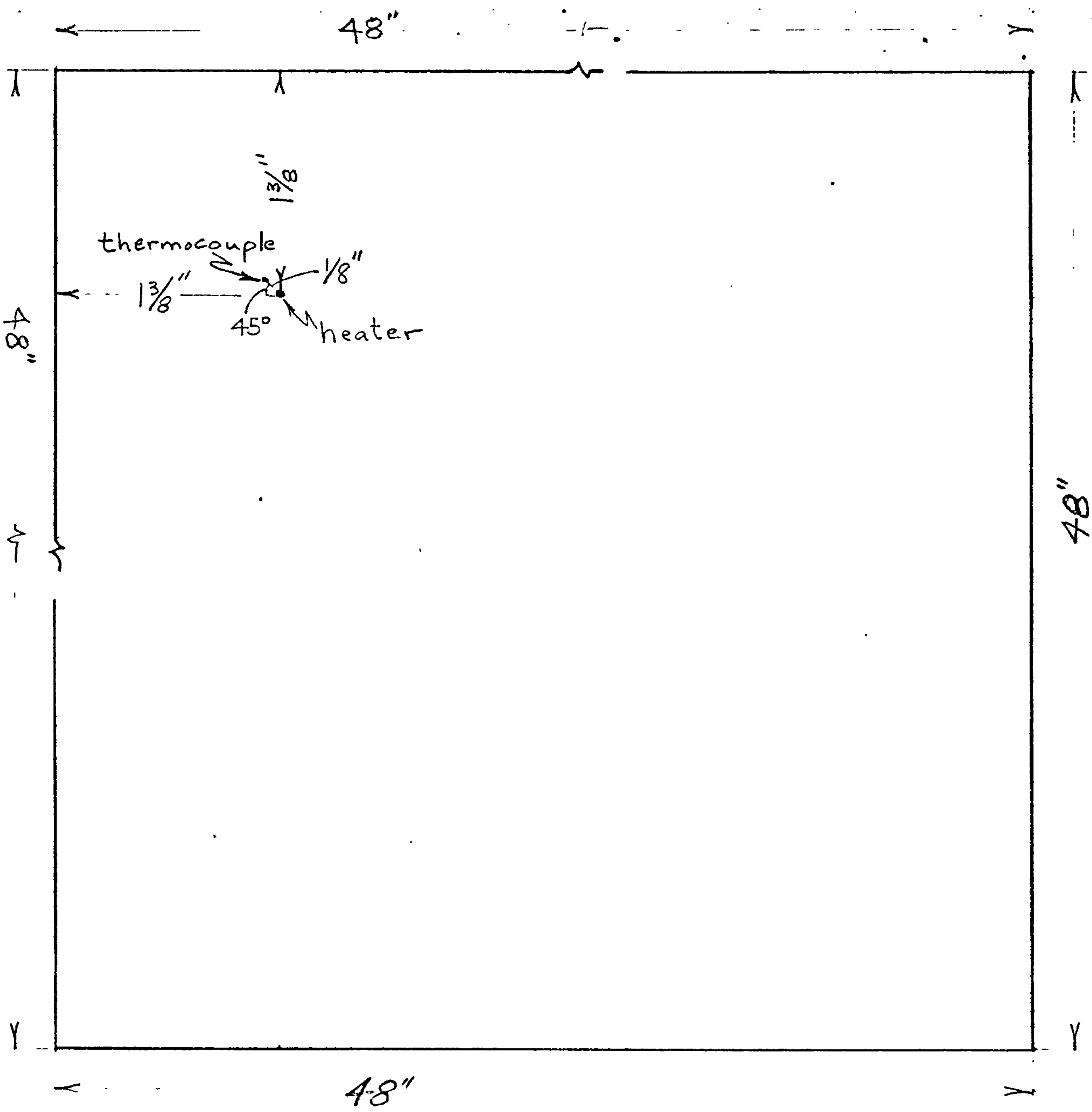

inch along the diagonal from the center of the heater well. The diameter of the heater well is approximately 3/32". This size heater was used in every case except the closed system case, where an one-eighth inch diameter heater was used as previously described.

The test results for this geometry using two different heat rates are presented in Figures 13 and 14 along with the expected ideal curves. The two heat rates used were 15 Btu/hr. and 2 Btu/hr. for the data in Figures 13 and 14, respectively. Both of these test runs were made using an ice bath as the thermocouple reference and an AC power supply as the drive for the heater.

Referring to both Figures 13 and 14, the results of the tests definitely lack the clear verification of the analytical solution that was present in the closed system case. For both heat rates, the early time data, i.e., before 3×10^{-3} hours, falls on a line which has a slope that is greater than that predicted by the analytical solution. The breaking off of the experimental data from this slope occurs at approximately the expected time, 3×10^{-3} hours, in both rate cases and the experimental data from approximately 5×10^{-2} hours falls on a line which has a slope almost exactly that of the ideal expected curve.

The behavior exhibited by the late time data in both heat rate cases, that is a correct slope value but data

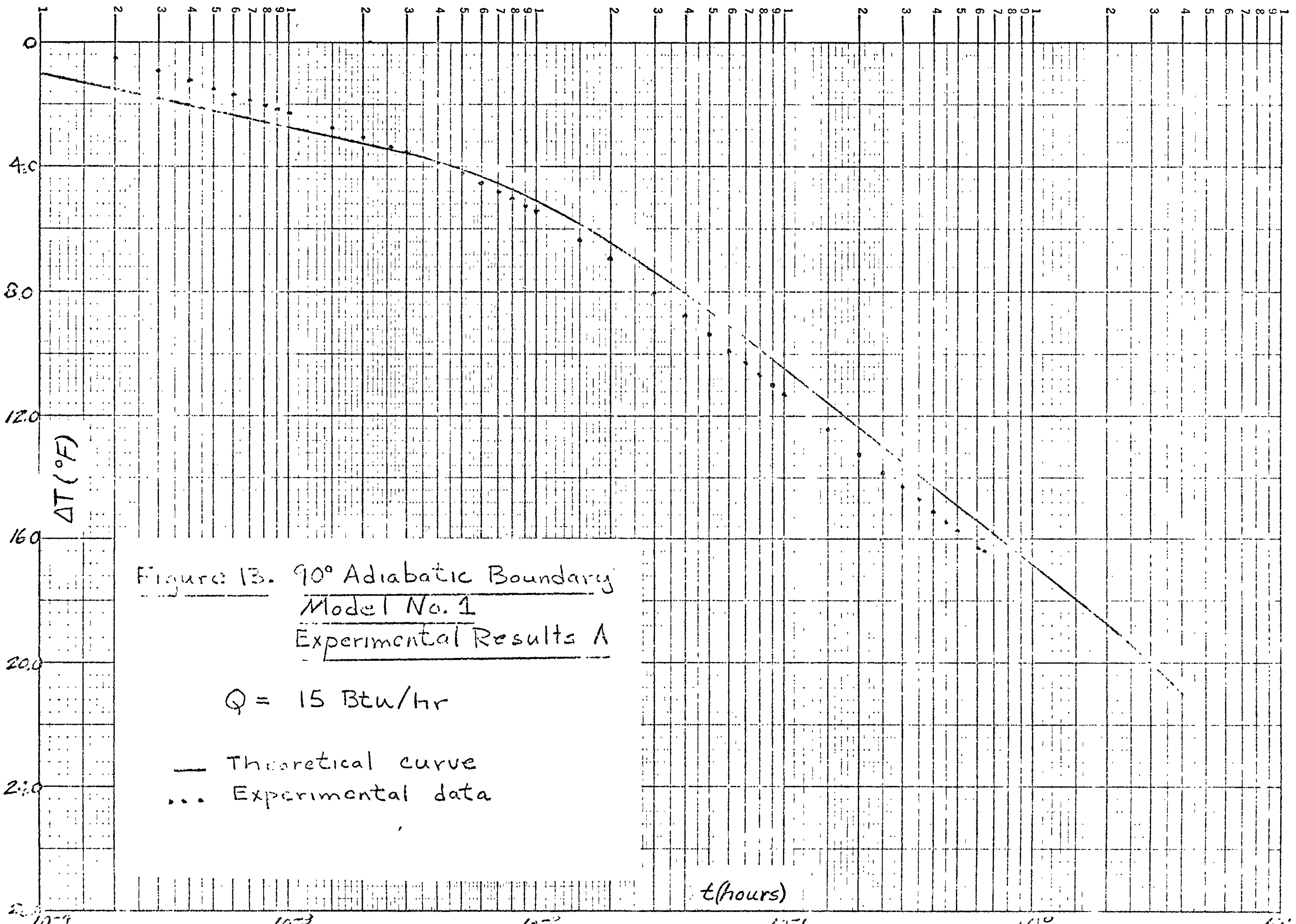
Figure 13. 90° Adiabatic Boundary
Model No. 1
Experimental Results A
Q = 15 Btu/hr
Theoretical curve
Experimental data
ΔT (°F)
t(hours)
0
4.0
8.0
12.0
16.0
20.0
10^{-4}
10^{-3}
10^{-2}
10^{-1}
10^{0}

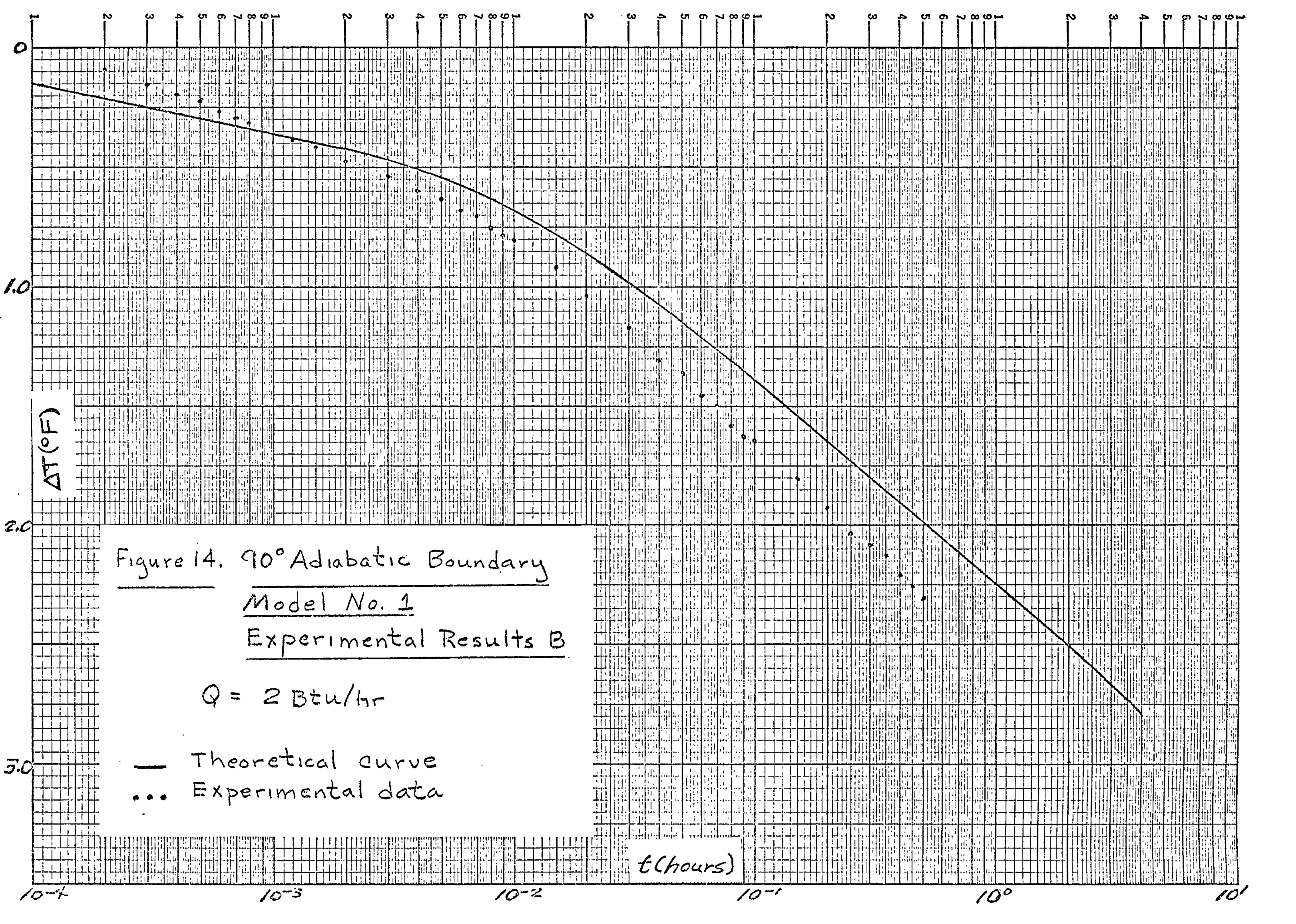

Figure 14. 90° Adiabatic Boundary
Model No. 1
Experimental Results B

points displaced a constant value above or below the ideal curve, is a relatively common occurrence in the petroleum reservoir. This behavior is caused by the presence of a "skin effect" around the wellbore and can be described in equation form as:

$$\Delta T = 4n \log \frac{2.25\alpha t}{\left[(r_w r_1 r_2 r_3)^2\right]^{1/4}} + \frac{SQ}{hk}$$

where the term $\frac{SQ}{hk}$ is the skin effect and S is called the skin. The skin may be positive or negative indicating an increase or decrease, respectively, in the buildup. This simply means that around the thermocouple there is an increase or decrease in the conductivity to allow for a larger or smaller temperature buildup.

In the heat conduction cases described in Figures 13 and 14, there would appear to be a positive skin if the late time data alone are considered, but this is not confirmed by the action of the early time data and such a positive skin is probably not physically possible under the described mechanical set-up. It seems more probable that the experimental results obtained were influenced by a geometry. effect related to the relative distances involved or as described below, a geometry effect unique to a specific case. Regardless, a positive skin is not a probable explanation for the observed phenomenon.

Another possible explanation could be that a geometry effect is present that is unique to the 90° adiabatic boundary case. If this is the case, then the above described behavior of the experimental data should be at least qualitatively repeatable in any other 90° boundary case regardless of the specific geometry.

In Figure 15, the geometry of another 90° adiabatic boundary case is illustrated. In this case the two nearest boundaries are at 2.88", the thermocouple well is .430" from the heater and instead of placing the thermocouple between the boundaries and the heater well, it is placed outside of that configuration. Although this represents a 90° adiabatic boundary case like the one shown in Figure 12, the distances between the heat well, the thermocouple and the adiabatic boundaries are changed and the thermocouple well was moved relative to the heat well.

The test results for the 90° case illustrated in Figure 15 using a 15 Btu/hr. heat rate, the electrical thermocouple reference and an AC power supply are plotted in Figure 16. These results compare quite favorably on a qualitative basis with the results presented for the 1.375"-90° boundary case with the late time data approaching the proper slope, data displaced below the ideal curve, and the early time data exhibiting a slope which is greater than the

Figure 15. 90° Adiabatic Boundary Model Geometry - Case No. 2

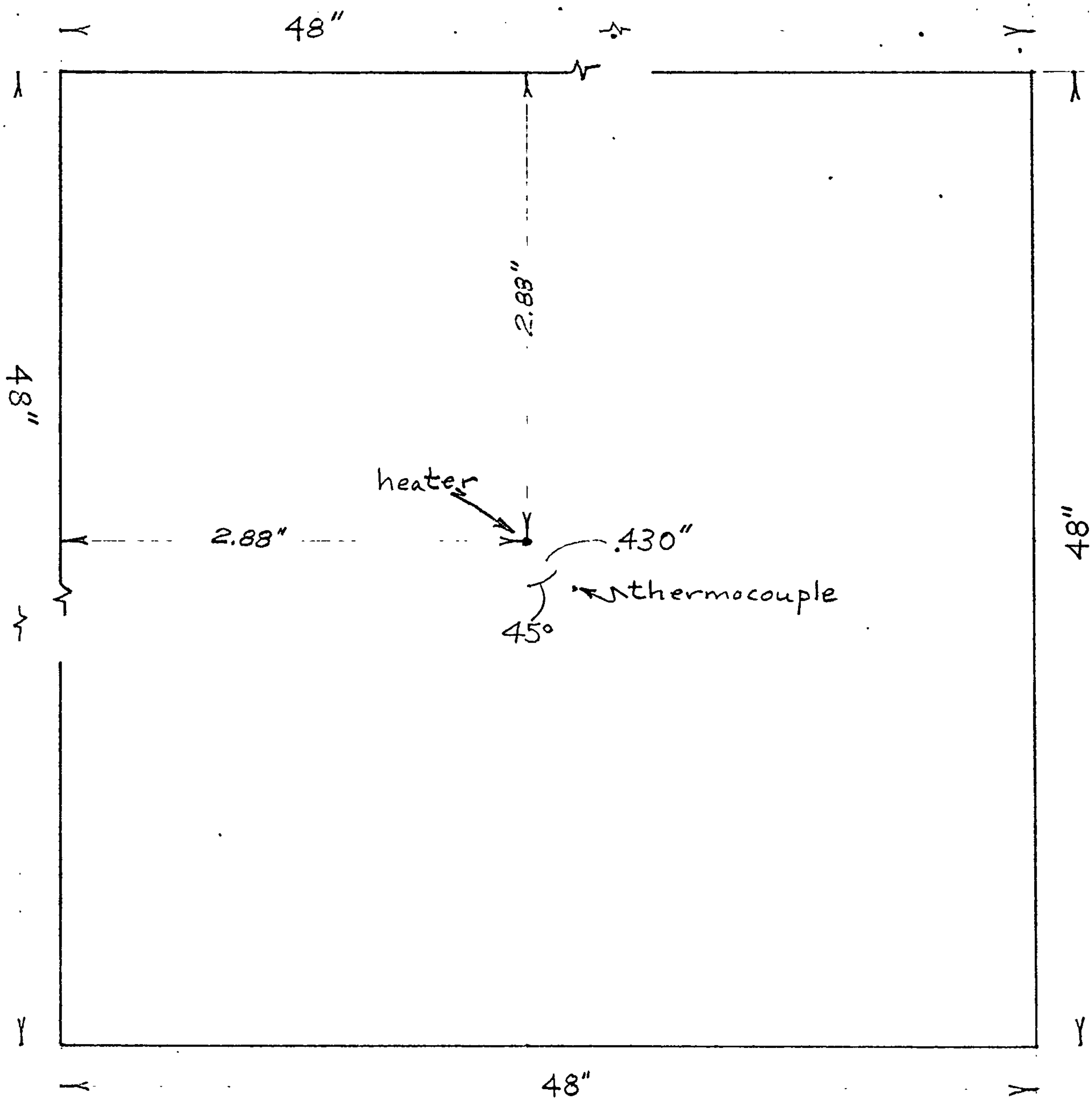

KEUFFEL & ESSER CO., N. Y. NO. 359-91
Semi-Logarithmic, 5 Cycles × 10 to the inch, 5th lines accented.
MADE IN U.S.A.

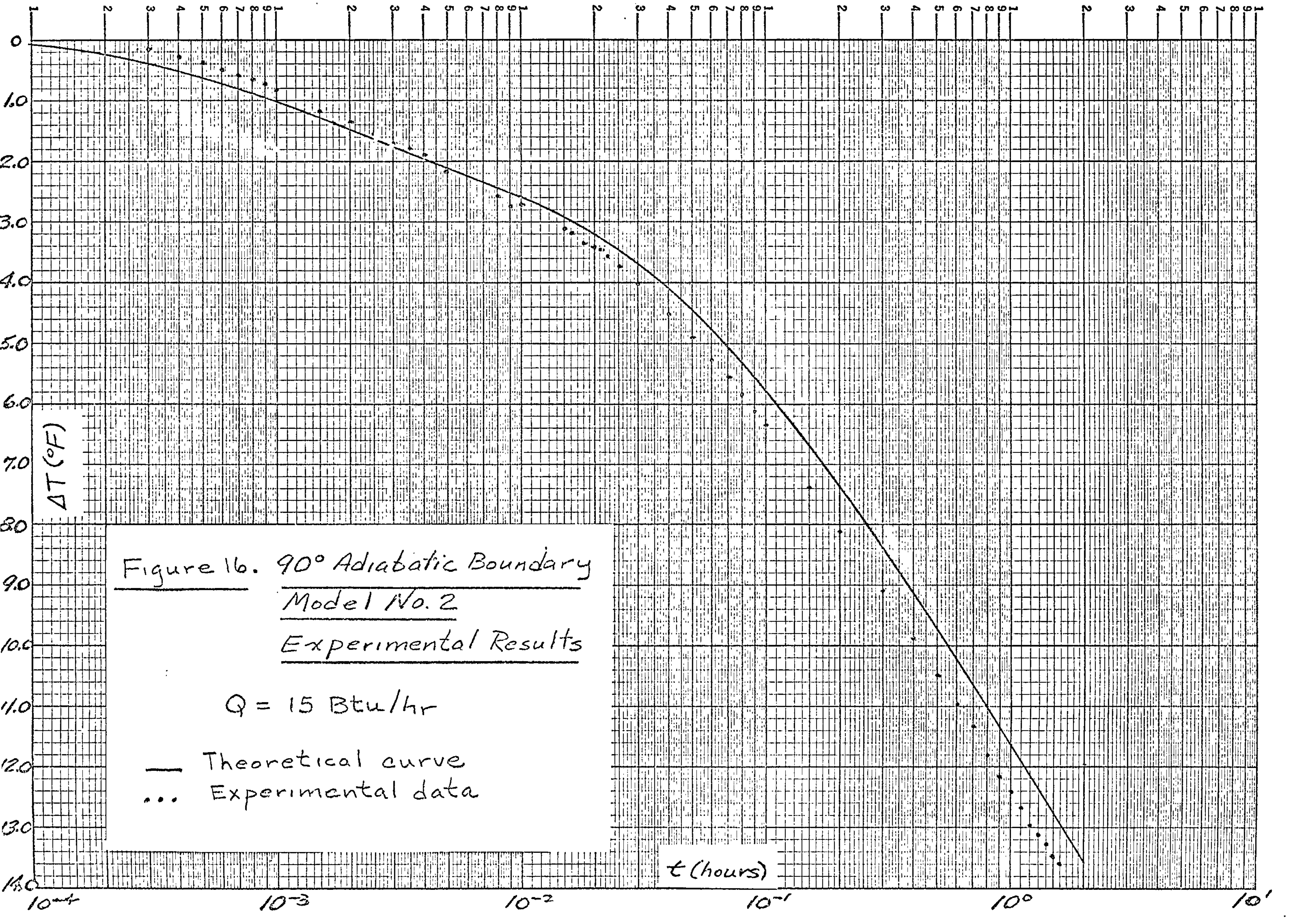

Figure 16. 90° Adiabatic Boundary Model No. 2 Experimental Results

expected slope value. This behavior lends some credence to the above stated idea that the experimental results could be effected by some geometry effect unique to a particular geometrical case.

180° Adiabatic Boundary.

Figure 17 illustrates the geometry of an 180° adiabatic boundary case where the fault is 1.375" from the heater well and the thermocouple well is approximately .18" from the heater on a 45° diagonal away from the adiabatic boundary.

The experimetal results using this model are illustrated in Figure 18. The electrical thermocouple reference, the AC power supply and a heat rate of approximately 14.8 Btu/hr. were used. The late time data approach the expected value of the slope with the data points being displaced above the ideal curve. Such behavior as described previously could be explained by a skin effect, in this case a negative skin. A negative skin could be expected due to the problems associated with the placement of the thermocouple but this hypothesis is not verified by the behavior of the early time data. Even so, the trend of the data after $1x10^{-3}$ hours is quite close to that of the ideal case with a skin effect.

Another explanation for the above described behavior, could be that the effect is unique to the 180° boundary

Figure 17. 180° Adiabatic Boundary Model Geometry - Case No. 1

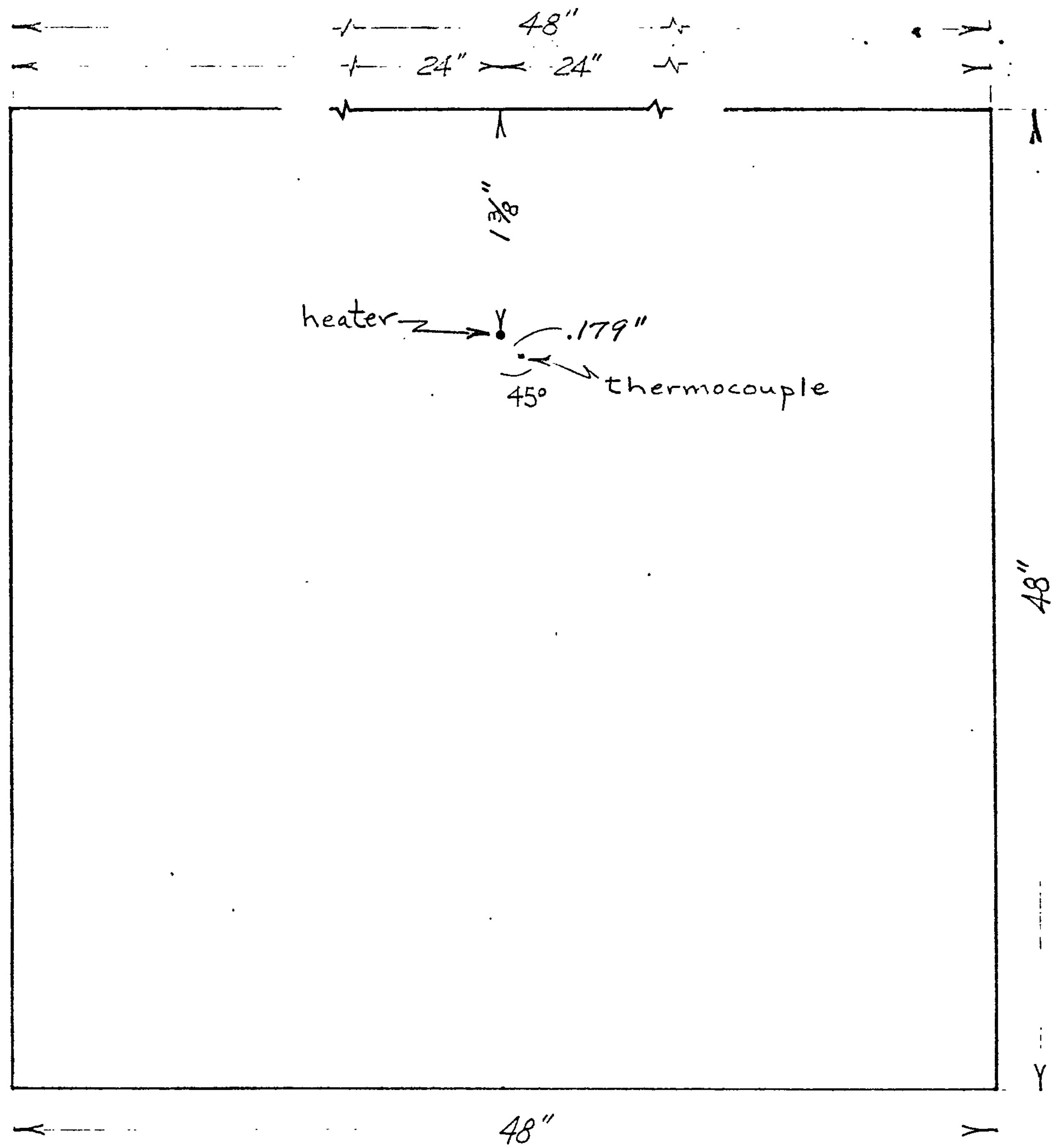

KEUFFEL & ESSER CO., N. Y. NO. 359-91
Semi-Logarithmic, 5 Cycles × 10 to the inch, 5th lines accented.
MADE IN U. S. A.

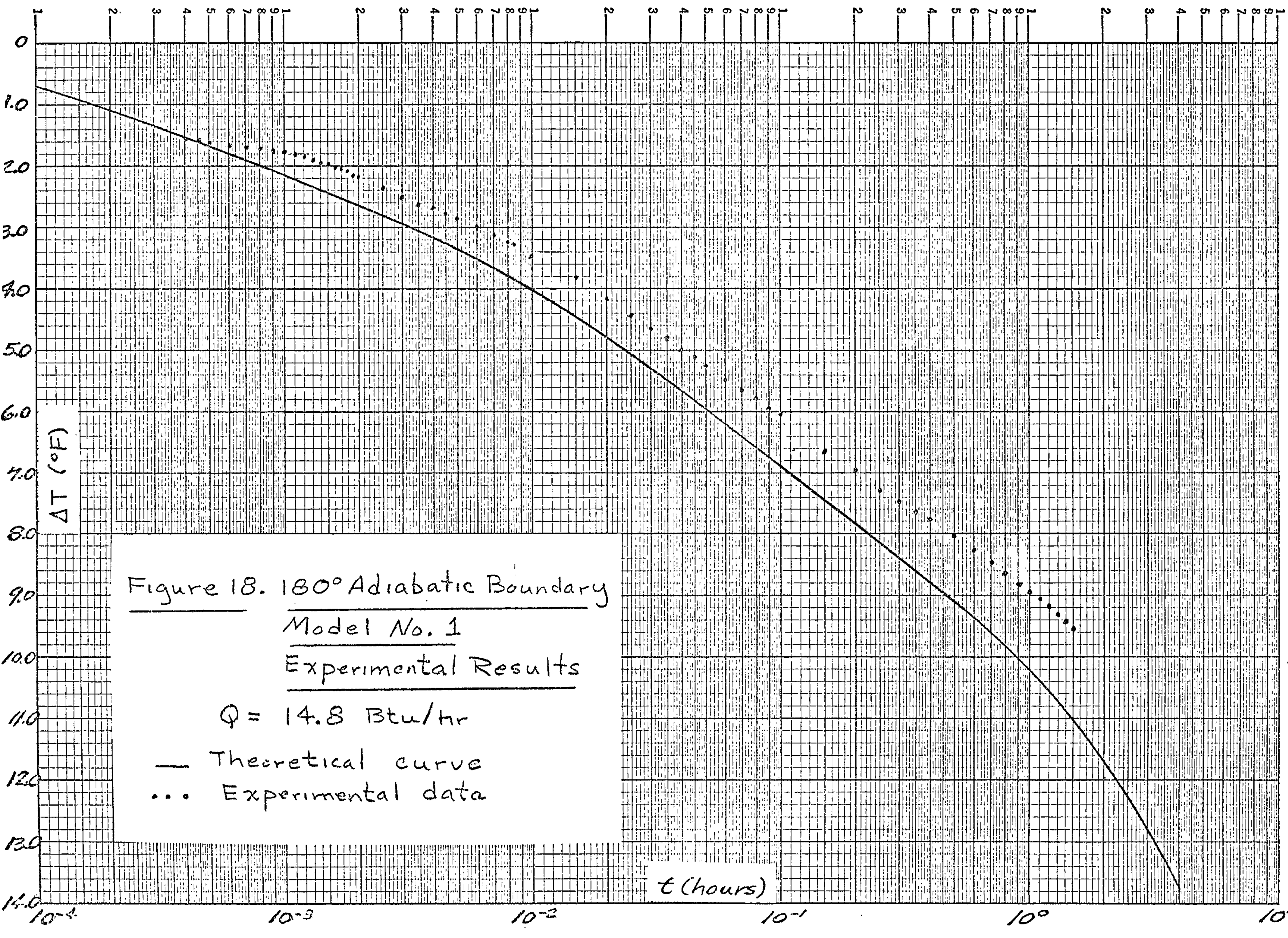

Figure 18. 180° Adiabatic Boundary
Model No. 1
Experimental Results

$Q = 14.8$ Btu/hr

— Theoretical curve
... Experimental data

geometry as described for the 90° boundary case. If this is the case, this behavior should be qualitatively repeatable on any other 180° boundary case.

A second 180° adiabatic boundary case is illustrated in Figure 19. For this case the boundary is 2.88" from the heater and the thermocouple is .430" away from the heater on a line parallel with the nearest adiabatic boundary.

The experimental results for the 2.88"-180° boundary model are illustrated in Figure 20 for the case where a heat flow rate of 17.4 Btu/hr. was used in conjunction with the electrical thermocouple reference and the AC power supply.

Although very early time data were not available, the test results seem to indicate the presence of a negative skin and this behavior compares quite favorably on a qualitative basis with the results obtained for the 1.375"-180° boundary model. This behavior tends to reinforce the idea stated in the section on 90° models that a geometry effect exists that is unique to the qualitative geometrical arrangement.

Figure 19. 180° Adiabatic Boundary Model Geometry.

Case No. 2

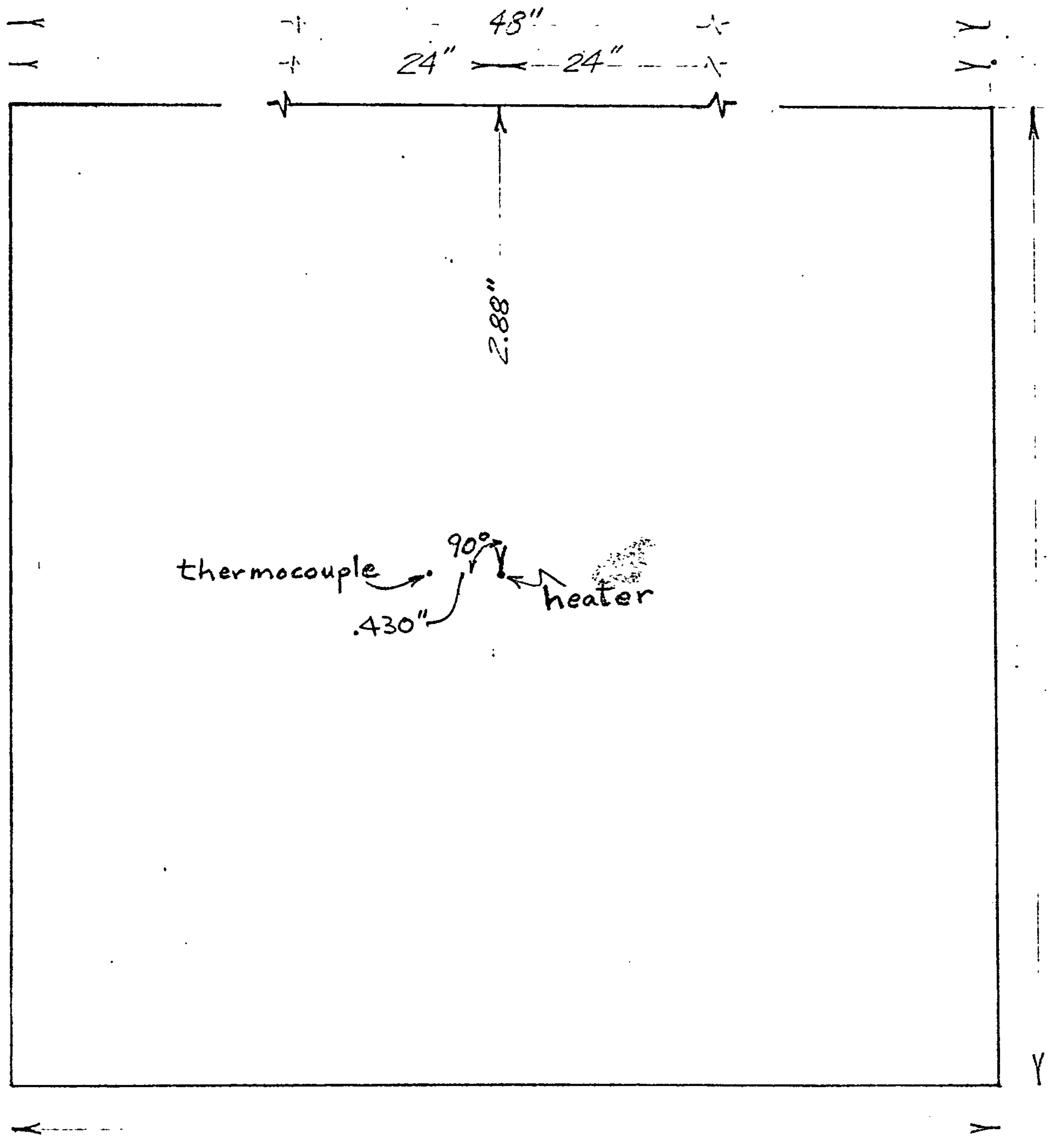

Semi-Logarithmic, 5 Cycles × 10 to the inch, 5th lines accented.
MADE IN U.S.A.

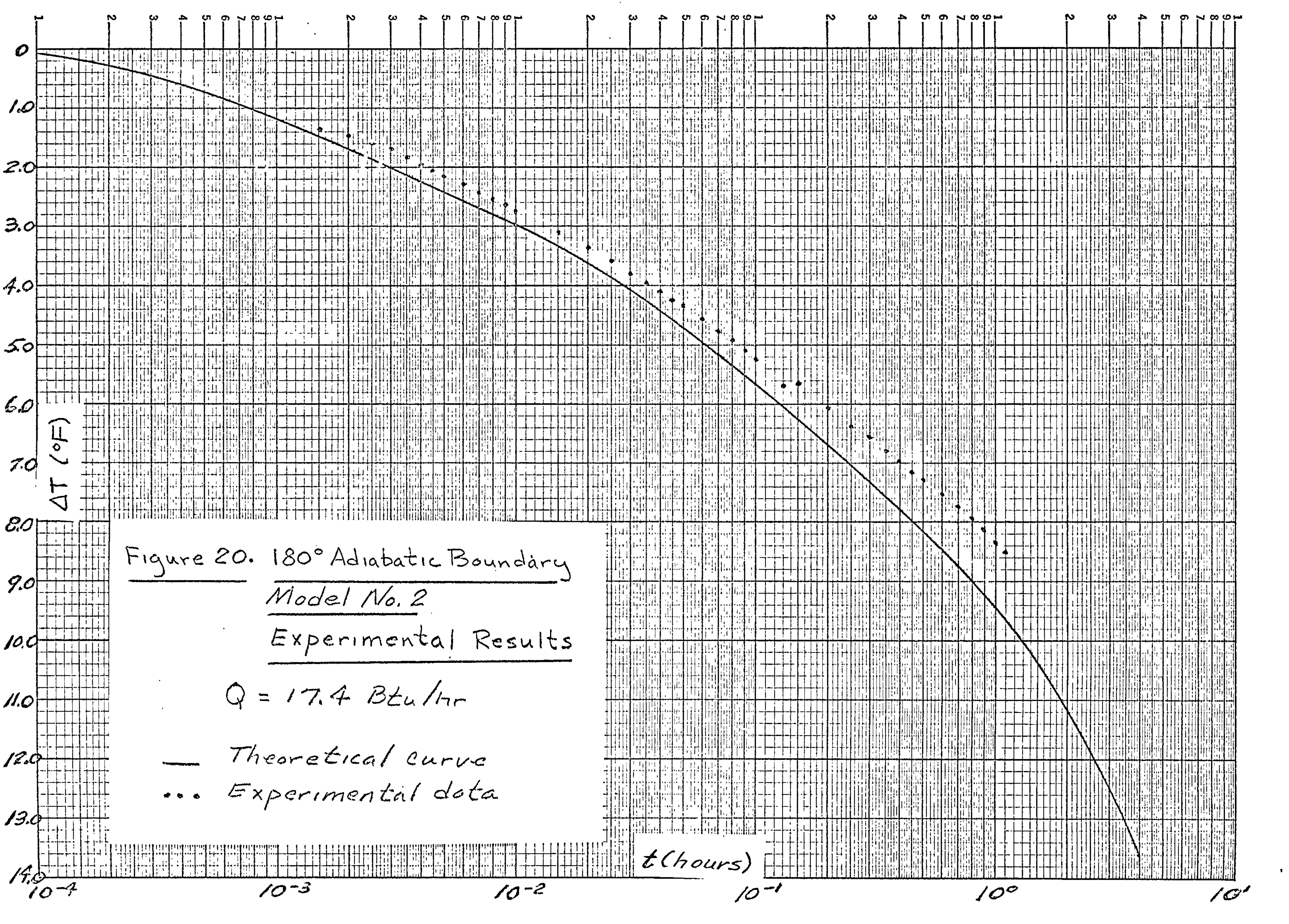

CHAPTER V

CONCLUSIONS AND RECOMMENDATIONS

The heat conduction model developed to experimentally verify the equations developed by the late Professor Park Jones in connection with transient pressure analysis in petroleum reservoirs has been partially successful. Specific positive results are noted. First, in all model cases the final expected slopes were approximated quite closely by the experimental results obtained. This would tend to indicate that the value of the slope calculated from the physical properties of the aluminum alloy and the calculated heat flow rate was correct.

Secondly, in all experimental cases the data underwent the expected changes in curve character at approximately the correct values of time. This behavior tends to indicate that the lack of ideal performance is due to geometrical effects.

In the third place, the experimental results first obtained for the closed system case verified the expected ideal solution within the limits of experimental accuracy. Similar results can be expected for the other geometrical cases studied once the pertinent parameters affecting the model performance for these cases are determined.

In light of the above stated positive factors the following conclusions and recommendations are made:

(1) Deviations in early time data are probably caused by geometrical borehole irregularities which result in distortions in the lines of heat flux from the ideal case and by small but significant time delays in thermocouple response because of the lack of intimate contact with the conducting material. The deviations should affect early time data more significantly than late time data due to (1) the magnitude of the temperature change, (2) the lack of other temperature transients (reflections) to reduce the distortions in the lines of heat flux and (3) the relative distance from the thermocouple to the wellbore.

(2) The overall lack of the heat conduction model performance to experimentally verify the expected ideal results in the 90° and 180° cases can be attributed primarily to the physical model not ideally representing the assumed mathematical model upon which the governing differential equation is based. This apparently results from such factors as geometrical irregularities in the boreholes, and the fact that all the distances involved, i.e., to faults and thermocouple to heatwell, were of relatively the same order of magnitude.

(3) It is suggested that in order to provide easier installation of heaters and thermocouples, in particular, that a granulated insulation be used. This should significantly reduce the time required to install the delicate thermocouples and heaters, and reduce movement of the insulation which can result in the breaking of the thermocouples and heaters.

(4) It is recommended that all electrical components be checked for accuracy and stability, including the electrical thermocouple reference, and that the grounding technique be refined to include a positive earth ground. Improvements in these areas could lead to reduced variations in recorded output due to mechanical shocks, stray electrical transients, and room temperature variations.

(5) The following experimental procedure is recommended as the starting point for defining the pertinent variables affecting model performance:

a. Using the closed system model, move the thermocouple from the 1" distance to a distance of 1/8" from the heatwell. Conduct the previously described experiment and, compare the results. This step should define the effect of this distance on the experimental results obtained and possibly help explain the behavior reported for the 90° and 180° adiabatic boundary cases.

b. In order to completely define the nature of the heat losses experienced by the model during a given experiment and to determine the effectiveness of the insulation in reducing these losses, conduct temperature buildup tests using each of the three geometrical cases without the upper layer of insulation. Then, conduct these same tests with the upper insulation in place and compare the results.

c. As a verification of the performance of the electrical thermocouple reference, conduct buildup tests with at least two different geometrical cases using this reference and then, repeat these same tests using a triple point reference. This procedure is recommended since in past experimental runs, the electrical thermocouple reference has appeared to be overly sensitive to temperature variations and mechanical shocks.

d. Sensitivity to mechanical shocks and temperature variations was also noted in the Sola Basic transformer that was used. It is recommended that a new one be obtained and temperature buildup tests conducted with both transformers to determine if the currently used transformer is too sensitive to external changes to be used in this work.

Before the heat conduction model used in this work can be used to experimentally verify the ideal solutions for more complicated geometrical systems than those investigated, or such variations as concentric areas of different thermal diffusivities, the model must be refined to be able to consistently reproduce the ideal solution for all cases discussed in this work. Once this is accomplished, the model will have great experimental value.

BIBLIOGRAPHY

BIBLIOGRAPHY

Craft, B. C. and M. F. Hawkins. Applied Petroleum Reservoir Engineering. New Jersey: Prentice-Hall, Inc., 1959.

Carslaw, H. C. and J. C. Jaeger. Conduction of Heat in Solids. London: Oxford University Press, 1959.

Hubbard, M. G. A Study of the Effect of Fluid Contacts on Transient Pressure Behavior in Homogeneous, Isotropic Porous Media. Master's Thesis, University of Houston, Houston, Texas, June, 1962.

Katz, M. L. Fluid Flow and Heat Transfer in Stratified Systems. Ph.D. Thesis, University of Michigan, Ann Arbor, Michigan, 1960

Matthews, C. S. and D. G. Russell. Pressure Buildup and Flow Tests in Wells. Dallas: AIME, 1967.

APPENDIX

APPENDIX A

PHYSICAL PROPERTIES

The values for the various physical properties of aluminum alloy #5052 used in the calculation of the ideal curves for each of the model cases discussed in Chapter IV are presented in this section. Substitution of these values in any of the equations describing transient temperature behavior along with the appropriate distance, time, and heat flow variables in inches, hours, and Btu/hr, respectively, results in temperature buildup in ^{o}F.

$$k = 6.6667 \text{ Btu/hr in } ^{o}F$$

$$c_p = .23 \text{ Btu/\#}^{o}F$$

$$\rho = 9.69 \times 10^{-2} \text{ \#/in}^3$$

$$\alpha = 299.13 \text{ in}^2\text{/hr}$$

APPENDIX B

EXPERIMENTAL AND CALCULATED DATA

Presented in this section for each of the experimental cases discussed in Chapter IV are the experimental data as taken from the strip chart record of each experiment and converted to temperature in ^{o}F. Also presented are the calculated values of temperature buildup which were used to plot the respective ideal curves.

Included with the above data for each model case are the exact ideal equations used to calculate the expected values of temperature buildup and the appropriate values of r which result from the image system required to describe transient temperature behavior over the period of time required for each experiment.

I. Closed System Model

Exact equation:

$$\Delta T = \frac{.183}{2.3}\frac{Q}{hk}\left[W\left(\frac{r_w^2}{4\alpha t}\right) + 2W\left(\frac{r_1^2}{4\alpha t}\right) + W\left(\frac{r_2^2}{4\alpha t}\right) + W\left(\frac{r_4^2}{4\alpha t}\right) + 2W\left(\frac{r_6^2}{4\alpha t}\right)\right.$$

$$\left. + 2W\left(\frac{r_8^2}{4\alpha t}\right) + 2W\left(\frac{r_{10}^2}{4\alpha t}\right) + 2W\left(\frac{r_{12}^2}{4\alpha t}\right) + 2W\left(\frac{r_{14}^2}{4\alpha t}\right) + 2W\left(\frac{r_{16}^2}{4\alpha t}\right)\right]$$

Experimental time: 2 hours

Values of r:

r_w = .9885"	r_8 = 68.5"
r_1 = 48.01"	r_{10} = 107.9"
r_2 = 48.99"	r_{12} = 108.2"
r_4 = 47.01"	r_{14} = 106.3"
r_6 = 67.2"	r_{16} = 107.0"

Heat Flow rate: 15.7 Btu/hr

Data:

t (hours)	ΔT (measured) (°F)	ΔT (calculated) (°F)
3.0×10^{-4}	0.00602	———
3.5 "	0.01263	———
4.0 "	0.01684	0.0346

t (hours)	ΔT (measured) (°F)	ΔT (calculated) (°F)
4.5×10^{-4}	0.02250	——
5.0 "	0.03067	——
6.0 "	0.05112	0.1197
7.0 "	0.07278	——
8.0 "	0.09985	0.1580
9.0 "	0.1239	——
1×10^{-3}	0.1546	0.2250
1.5 "	0.3013	——
2.0 "	0.4668	0.513
2.5 "	0.5522	——
3.0 "	0.6574	——
4.0 "	0.8553	0.8978
4.5 "	0.9588	——
5.5 "	1.079	——
6.0 "	1.134	1.238
7.0 "	1.240	——
8.0 "	——	1.343
9.0 "	1.439	——
1.0×10^{-2}	1.501	1.494
1.5 "	1.774	——
1.9 "	1.942	——
2.0 "	——	1.980
2.5 "	2.163	——
3.0 "	2.281	——
4.0 "	2.507	2.480
4.5 "	2.616	——
6.0 "	2.846	2.872
7.0 "	2.927	——
8.0 "	3.044	2.988
9.0 "	3.153	——
1.0×10^{-1}	3.206	3.152
1.5 "	3.559	——
2.0 "	3.725	3.664
2.5 "	3.859	——
3.0 "	4.017	——
4.0 "	4.216	4.182
5.0 "	4.391	——
6.0 "	4.571	4.606
7.0 "	4.713	——
7.8 "	4.845	——
8.0 "	4.786	4.781
9.0 "	4.920	——
1.0×10^{0}	5.023	5.034
1.1 "	5.143	——

t (hours)	ΔT (measured) (^oF)	ΔT (calculated) (^oF)
$1.2x10^0$	5.237	———
1.3 "	5.318	———
1.4 "	5.421	———
1.5 "	5.526	———
1.6 "	5.665	———
1.7 "	5.762	———
1.8 "	5.859	———
1.9 "	5.993	———
2.0 "	6.082	6.237
2.1 "	6.192	———
2.2 "	6.335	———
2.25 "	6.416	———

II. 90° Adiabatic Boundary Models

Exact equation:

$$\Delta T = \frac{.183}{2.3}\frac{Q}{hk}\left[W\left(\frac{r_w^2}{4\alpha t}\right) + 2W\left(\frac{r_1^2}{4\alpha t}\right) + W\left(\frac{r_3^2}{4\alpha t}\right)\right]$$

Experimental time: 2 hours

Values of r:

Case No. 1

r_w = .125" r_1 = 2.66" r_3 = 3.76"

Case No. 2

r_w = .430" r_1 = 6.07" r_3 = 8.57"

Heat Flow rate:

Case No. 1-A - - 15 Btu/hr

Case No. 1-B - - 2 Btu/hr

Case No. 2 - - 15 Btu/hr

Data Case No. 1-A:

t (hours)	ΔT (measured) (°F)	ΔT (calculated) (°F)
2.0×10^{-4}	0.484	1.581
3.0 "	0.895	———
4.0 "	1.216	2.045
5.0 "	1.469	———
6.0 "	1.673	2.325
7.0 "	1.861	———
8.0 "	2.018	2.526
9.0 "	2.160	———

t (hours)	ΔT (measured) (°F)	ΔT (calculated) (°F)
1.0×10^{-3}	2.278	2.682
1.5 "	2.765	——
2.0 "	3.092	3.190
2.6 "	3.364	——
3.0 "	3.549	——
4.0 "	3.935	3.817
5.0 "	4.234	——
6.0 "	4.555	4.303
7.0 "	4.811	——
8.0 "	5.060	4.718
9.0 "	5.296	——
1.0×10^{-2}	5.463	5.083
1.5 "	6.358	——
2.0 "	6.942	6.433
3.0 "	8.027	——
4.0 "	8.746	8.044
5.0 "	9.370	——
6.0 "	9.882	9.069
7.0 "	10.265	——
8.0 "	10.672	9.821
9.0 "	11.006	——
1.0×10^{-1}	11.320	10.414
1.5 "	12.438	——
2.0 "	13.277	12.302
2.5 "	13.825	——
3.0 "	14.299	——
3.5	14.715	——
4.0 "	15.114	14.232
4.5 "	15.456	——
5.0 "	15.715	——
6.0 "	16.246	15.371
6.4 "	16.394	——
8.0 "	——	16.180
1.0×10^{-0}	——	16.810
2.0 "	——	18.788

Data Case No. 1-B:

t (hours)	ΔT (measured) (°F)	ΔT (calculated) (°F)
2.0×10^{-4}	0.089	0.211
3.0 "	0.151	——
4.0 "	0.196	0.273

t (hours)	ΔT (measured) (°F)	ΔT (calculated) (°F)
5.0×10^{-4}	0.222	——
6.0 "	0.269	0.310
7.0 "	0.273	——
8.0 "	0.314	0.337
1.0×10^{-3}	——	0.358
1.2 "	0.389	——
1.5 "	0.417	——
2.0 "	0.473	0.425
3.0 "	0.541	——
4.0 "	0.602	0.509
5.0 "	0.636	——
6.0 "	0.680	0.574
7.0 "	0.705	——
8.0 "	0.751	0.629
9.0 "	0.781	——
1.0×10^{-2}	0.804	0.678
1.5 "	0.920	——
2.0 "	1.036	0.858
3.0 "	1.170	——
4.0 "	1.302	1.073
5.0 "	1.353	——
6.0 "	1.457	1.209
7.0 "	1.500	——
8.0 "	1.580	1.309
9.0 "	1.627	——
1.0×10^{-1}	1.642	1.388
1.5 "	1.802	——
2.0 "	1.926	1.640
2.5 "	2.033	——
3.0 "	2.083	——
3.5 "	2.128	——
4.0 "	2.212	1.898
4.5 "	2.259	——
5.0 "	2.308	——
6.0 "	——	2.050
8.0 "	——	2.157
1.0×10^{-0}	——	2.241

Data Case No. 2:

t (hours)	ΔT (measured) (°F)	ΔT (calculated) (°F)
3.0×10^{-4}	0.150	——
4.0 "	0.268	0.516

t (hours)	ΔT (measured) (^oF)	ΔT (calculated) (^oF)
5.0×10^{-4}	0.375	—
6.0 "	0.490	0.726
7.0 "	0.586	—
8.0 "	0.656	0.889
9.0 "	0.734	—
1.0×10^{-3}	0.834	1.022
1.5 "	1.191	—
2.0 "	1.365	1.463
2.5 "	1.561	—
3.0 "	1.708	—
3.5 "	1.785	—
4.0 "	1.901	1.928
5.0 "	2.183	—
6.0 "	—	2.209
8.0 "	2.598	2.414
9.0 "	2.749	—
1.0×10^{-2}	2.695	2.581
1.5 "	3.128	—
1.6 "	3.188	—
1.8 "	3.374	—
2.0 "	3.417	3.193
2.1 "	3.465	—
2.25 "	3.579	—
2.50 "	3.729	—
3.0 "	4.078	—
4.0 "	4.499	4.074
5.0 "	4.896	—
6.0 "	5.263	4.751
7.0 "	5.528	—
8.0 "	5.834	5.300
9.0 "	6.111	—
1.0×10^{-1}	6.340	5.749
1.5 "	7.380	—
2.0 "	8.108	7.362
3.0 "	9.079	—
4.0 "	9.865	9.131
5.0 "	10.478	—
6.0 "	10.959	10.216
7.0 "	11.320	—
8.0 "	11.811	10.999
9.0 "	12.162	—
1.0×10^{-0}	12.403	11.610
1.1 "	12.668	—
1.2 "	12.956	—

t (hours)	ΔT (measured) (^{o}F)	ΔT (calculated) (^{o}F)
1.3×10^{-0}	13.125	——
1.4 "	13.281	——
1.5 "	13.486	——
1.6 "	13.600	——
2.0 "	——	13.559

III. 180° Adiabatic Boundary Models

Exact equation:

$$\Delta T = \frac{.183}{2.3}\frac{Q}{hk}\left[W\left(\frac{r_w^2}{4\alpha t}\right) + W\left(\frac{r_1^2}{4\alpha t}\right) + W\left(\frac{r_2^2}{4\alpha t}\right) + W\left(\frac{r_3^2}{4\alpha t}\right) + W\left(\frac{r_4^2}{4\alpha t}\right) + W\left(\frac{r_5^2}{4\alpha t}\right)\right]$$

Experimental time: 2 hours

Values of r:

Case No. 1

r_w = .179"	r_3 = 48.13"
r_1 = 2.88"	r_4 = 47.90"
r_2 = 47.87"	r_5 = 48.24"

Case No. 2

r_w = .430"	r_3 = 47.57"
r_1 = 5.77"	r_4 = 48.70"
r_2 = 48.43"	r_5 = 47.85"

Heat Flow rate:

Case No. 1 - - 14.8 Btu/hr

Case No. 2 - - 17.4 Btu/hr

Data Case No. 1:

t (hours)	ΔT (measured) (°F)	ΔT (calculated) (°F)
4×10^{-4}	1.546	1.535
4.5 "	1.588	———

t (hours)	ΔT (measured) (°F)	ΔT (calculated) (°F)
5.0×10^{-4}	1.609	——
6.0 "	1.663	1.803
7.0 "	1.684	——
8.0 "	1.708	1.997
9.0 "	1.732	——
1.0×10^{-3}	1.780	2.149
1.1 "	1.813	——
1.2 "	1.844	——
1.3 "	1.901	——
1.4 "	1.930	——
1.5 "	1.961	——
1.6 "	2.027	——
1.7 "	2.045	——
1.8 "	2.075	——
1.9 "	2.144	——
2.0 "	2.171	2.629
2.5 "	2.370	——
3.0 "	2.502	——
3.5 "	2.610	——
4.0 "	2.680	3.155
4.5 "	2.767	——
5.0 "	2.845	——
6.0 "	2.989	3.505
7.0 "	3.116	——
8.0 "	3.224	3.781
8.5 "	3.254	——
1.0×10^{-2}	3.447	4.008
1.5 "	3.817	——
2.0 "	4.174	4.787
2.5 "	4.427	——
3.0 "	4.652	——
3.5 "	4.784	——
4.0 "	4.998	5.650
4.5 "	5.115	——
5.0 "	5.256	——
6.0 "	5.474	6.179
7.0 "	5.630	——
8.0 "	5.774	6.563
9.0 "	5.925	——
1.0×10^{-1}	6.027	6.863
1.5 "	6.647	——
2.0 "	6.935	7.809
2.5 "	7.254	——
3.0 "	7.453	——
3.5 "	7.639	——

t (hours)	ΔT (measured) (^{o}F)	ΔT (calculated) (^{o}F)
4.0×10^{-1}	7.765	8.772
5.0 "	8.024	—
6.0 "	8.259	9.357
7.0 "	8.453	—
8.0 "	8.631	9.810
9.0 "	8.812	—
1.0×10^{-0}	8.944	10.193
1.1 "	9.065	—
1.2 "	9.179	—
1.3 "	9.311	—
1.4 "	9.426	—
1.5 "	9.534	—
2.0 "	—	11.673

Data Case No. 2:

t (hours)	ΔT (measured) (^{o}F)	ΔT (calculated) (^{o}F)
1.0×10^{-3}	1.192	1.185
1.5 "	1.335	—
2.0 "	1.449	1.697
2.5 "	1.578	—
3.0 "	1.684	—
3.5 "	1.826	—
4.0 "	1.949	2.237
4.5 "	2.045	—
5.0 "	2.147	—
6.0 "	2.286	2.563
7.0 "	2.408	—
8.0 "	2.526	2.799
9.0 "	2.633	—
1.0×10^{-2}	2.731	2.988
1.5 "	3.086	—
2.0 "	3.344	3.633
2.5 "	3.573	—
3.0 "	3.771	—
3.5 "	3.934	—
4.0 "	4.084	4.412
4.5 "	4.241	—
5.0 "	4.307	—
6.0 "	4.539	4.933
7.0 "	4.764	—
8.0 "	4.900	5.327

t (hours)	ΔT (measured) (°F)	ΔT (calculated) (°F)
9.0 "	5.077	—
1.0×10^{-1}	5.227	5.628
1.5 "	5.630	—
2.0 "	6.075	6.682
2.5 "	6.370	—
3.0 "	6.514	—
3.5 "	6.779	—
4.0 "	6.977	7.774
4.5 "	7.146	—
5.0 "	7.256	—
6.0 "	7.525	8.451
7.0 "	7.735	—
8.0 "	7.946	8.980
9.0 "	8.132	—
1.0×10^{-0}	8.337	9.422
1.1 "	8.481	—
2.0 "	—	11.161

APPENDIX C

NOMENCLATURE

<u>For Fluid Flow</u>

A	=	Cross-sectional area, square feet.
a	=	Distance to a fault, feet.
b	=	Distance to a fault, feet.
c	=	Fluid compressibility, psi^{-1}
D	=	Reservoir resistivity, $\frac{\mu}{1.127(2\pi)h\,k}$, psi/bbl/day.
d	=	Distance to a fault, feet
h	=	Formation thickness, feet.
j	=	Pressure drawdown, psi.
k	=	Permeability, darcies.
m	=	Slope of drawdown vs. log time curve, psi/log cycle.
P	=	Reservoir pressure, psia.
P_i	=	Initial reservoir pressure, psia.
q	=	Volumetric reservoir flow rate, bbl/day.
q''	=	Volumetric reservoir flow flux, bbl/day-ft.^{2}
r	=	Radial distance from wellbore or image well; feet.
r_w	=	Radius of wellbore, feet.
t	=	Time, days.
t_o	=	Time intercept of the straight line portions of the drawdown vs. log time curve, days.
x	=	Cartesian co-ordinate direction, feet.
y	=	Cartesian co-ordinate direction, feet.

Greek Letters

η	=	Formation diffusivity, $\frac{6.328\ k}{\mu \phi c}$, square feet/day
θ	=	Time intercept of first linear portion of drawdown vs. log time curve at j = 0, days.
ρ	=	Fluid density, lb-mass/cubic foot.
ρ_o	=	Initial density, lb-mass/cubic foot.
μ	=	Fluid viscosity, centipoise.
ϕ	=	Formation porosity, draction.

For Heat Conduction

a	=	Distance to adiabatic boundary, inches.
b	=	Distance to adiabatic boundary, inches.
c_p	=	Heat capacity, Btu/lb-^oF
d	=	Distance to adiabatic boundary, inches.
f	=	Heat flux, Btu/hr-square inch.
h	=	Thickness of heat conducting medium, inches.
k	=	Thermal conductivity, Btu/hr-inch^oF.
n	=	Slope of temperature drawdown vs. log time curve, ^oF/log cycle.
Q	=	Heat flow rate, Btu/hr.
r	=	Radial distance from heat well or from image well, inches.
r_w	=	Radius of heat well or from heat well to observation point, inches.
T	=	Temperature, ^oF.
ΔT	=	Temperature drawdown (or buildup), ^oF.
t	=	Time, hours.
x	=	Cartesian co-ordinate direction, inches.
y	=	Cartesian co-ordinate direction, inches.

Greek Letters

α	=	Thermal diffusivity, $\frac{k}{\rho c_p}$, square inches/hr.
θ	=	Time intercept of first linear portion of temperature drawdown curve at $T = 0$, hours.
ρ	=	Density of heat conducting medium, lb-mass/cubic foot.